ABSTRACT

Title of Document:
PROTOTYPE DESIGN FOR
THERMOACOUSTIC FLASHOVER DETECTOR

Krystyna Eva Buda-Ortins
Master of Science, 2012

Directed By:
Dr. Peter Sunderland, Associate Professor
Department of Fire Protection Engineering

The thermoacoustic flashover detector integrates the phenomenon of thermoacoustics into a fire fighting application. This report presents the prototype design for the thermoacoustic flashover detector to ultimately be implemented in a firefighter's gear. Upon increases in compartment fire heat flux and temperature corresponding to the onset of flashover, the device will produce a loud warning tone to alert the firefighter that flashover is impending. This is critical because post-flashover, the fire transitions to an untenable environment for a firefighter, as well as compromised structural integrity of the building. The current design produces a tone at 115 dB at about 500 Hz upon heating from an external band heater and cooling via an ice/water bath. At 38 mm from the device, this sound level is louder than the 85 dB from fire alarms and distinct from the 3000 Hz tone of smoke detectors. The minimum power input to the device for sound onset is 44 W, corresponding to a temperature difference of 150 ℃ at a mean temperature of 225 ℃ across a 2 cm long porous steel wool stack. The temperatures at the hot and cold ends of the stack are 300 ℃ and 150 ℃ respectively, which is achieved with a response time of ~100 seconds. The sound is sustained as long as there is a minimum power input of 31 W. Although the measurement uncertainties are estimated at ± 10 ℃ for the temperatures and ± 5 W for the power input, this design provides a foundation for future improvement and quantification of the device. The mechanisms of the thermoacoustics at work and the materials selected for the prototype are presented. Different power level inputs to the device are analyzed and temperatures for operation are determined. Suggestions for future optimization and integration of the device into firefighters' gear are presented.

PROTOTYPE DESIGN FOR THERMOACOUSTIC FLASHOVER DETECTOR

By

Krystyna Eva Buda-Ortins

Thesis submitted to the Faculty of the Graduate School of the
University of Maryland, College Park, in partial fulfillment
of the requirements for the degree of
Master of Science
2012

Advisory Committee:
Associate Professor Peter Sunderland, Chair
Professor Emeritus James G. Quintiere
Professor Amr Baz
Professor Marino diMarzo

ACKNOWLEDGEMENTS

I would like to thank the faculty in the Fire Protection Engineering department for teaching me so much in the past five years. I would especially like to thank my advisor Dr. Sunderland for supporting and guiding me in this project, and my project team including Dr. diMarzo, Dr. Quintiere and Dr. Baz. You all have had great, innovative ideas during the project and the design has come a long way thanks to all your brainstorming and simplification. Dr. Milke, thank you for recruiting me to FPE back when I was in high school—it was one of the best decisions I have made in my life.

I would like to thank Olga for all her help in the lab, and all the students who have assisted me from time to time. Ken, thank you for all your assistance in the lab through many trials and errors, and finally to a working prototype. You always have had practical ideas and solutions to design issues.

Mostafa, thank you for taking the time to explain thermoacoustics to me time after time, making sure that I understand the concepts, and pointing me in directions toward useful literature. You've helped me tremendously in understanding my research and in building a working design.

I would not be the happy camper that I am without the day-to-day interactions with the staff in the Fire Protection Engineering department. Sharon, Mary Lou and Pat, you all have made the past five years sunny and provided me with so many smiles and laughs. I will miss you immensely when I move on to the big world.

Of course, thank you to my parents for encouraging me to be an engineer and cheering me on over the years. Thank you Doug, for always listening and simplifying any kind of problem I can throw at you. Thanks to all my friends who have been here to keep me laughing.

TABLE OF CONTENTS

LIST OF TABLES

LIST OF FIGURES

NOMENCLATURE

A Cross-sectional area
ID Inner diameter
L Resonator length
M Mass
OD Outer diameter
P Power
$\dot{Q}$ Heat
R Gas constant
$Re[z]$ Real part of z
T Temperature
ΔT Temperature difference
∇T Temperature gradient
U_1 Velocity amplitude
V Volume

c_p Specific heat per unit mass at constant pressure
i Imaginary number: $\sqrt{-1}$
k Thermal conductivity
l Half of plate thickness in stack
y_0 Half of plate spacing in stack
p_1 Pressure amplitude
p_m Mean pressure
r_h Hydraulic radius
t Time
x Space coordinate parallel to acoustic motion (x=0 corresponds to closed end)
x_1 Gas displacement amplitude
Δx Stack length
x_{stack} X-coordinate of center of stack

Subscripts
hot Hot end
hx Heat exchanger
$cold$ Cold end
m Mean
$onset$ Onset of sound
ss Steady-state
$stack$ Stack property

Greek letters

a Speed of sound

f Oscillation frequency

γ Ratio of specific heats

κ Thermal diffusivity

λ Wavelength of sound wave

δ_κ Thermal penetration depth

δ_υ Viscous penetration depth

μ Dynamic viscosity

ρ Density

σ Prandtl number

υ Kinematic viscosity

ω Angular frequency

1. Introduction

1.1. The Thermoacoustic Flashover Detector

Flashover and structural collapse contribute to a significant amount of firefighter fatalities and injuries. Every year, 100 firefighters are killed and 100,000 are injured in the line of duty [1]. Within the protective turnout gear of a firefighter, it is often difficult to judge when flashover is imminent, especially with poor visibility due to thick smoke and improvements in thermal resistance of firefighter gear.

The thermoacoustic flashover detector will ultimately be a passive helmet-mounted alarm that audibly alerts firefighters to conditions of pending flashover. Upon impending flashover, a thermal gradient and heat input from the fire environment to the device will produce a thermoacoustic sound wave. This loud tone propagating from the device will alert firefighters when flashover is approaching. It will be powered by the radiant heat from the smoke layer of the fire, and involves no electronics, batteries or moving parts. This system will significantly improve firefighter safety and effectiveness by identifying impending flashover.

The design presented here is a prototype that produces a tone based on a heat input to the device, simulating the heat collected from the impending flashover in a real fire scenario. Further improvements to this design allow it to be calibrated and reduced in size to meet the ultimate design criteria.

1.1.1. Flashover

Enclosure fires typically develop in three stages: growth, fully-developed burning, and decay. A plot of temperature versus time for a typical uncontrolled compartment fire is shown in Figure 1-1.
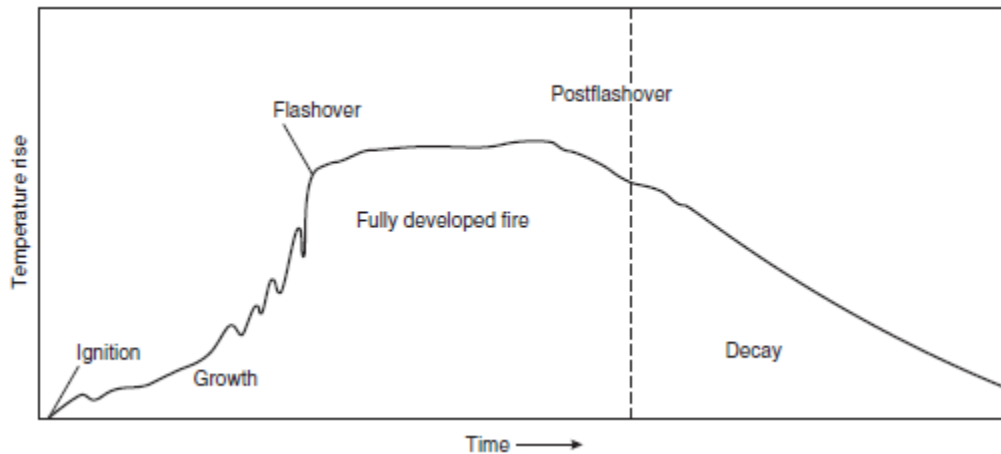
Figure 1-1. Temperature vs. time in a typical uncontrolled compartment fire. [3].

After ignition, the fire may grow at a slow or a fast rate, depending on the type of fuel, interaction with surroundings, and access to oxygen. This stage is usually fuel limited, as there is plenty of oxygen available but the combustibles need to heat up and pyrolize before they can contribute to the fire. If the fuel is flammable enough, the fire may grow at a rapid rate where the heat flux from the initial burning item is sufficient to ignite adjacent fuel.

In the fully-developed burning stage, the heat release rate and temperatures within the room are at their greatest. The fire is often limited by the availability of oxygen entering through the openings such as windows or doors. This stage may last for hours as long as there is sufficient fuel and oxygen. In this

stage, unburnt gases can collect at the ceiling level only to ignite upon the introduction of oxygen, and the flames may extend out of openings as the fire seeks air [4]. The average gas temperature in the enclosure during this stage is in the range of $700 - 1200\ ℃$ and may substantially weaken structural components of the room, endangering nearby occupants or firefighters. As the fuel becomes consumed, the fire reaches the third stage, decay, in which the fire is fuel limited as it dies out [5].

As the upper layer temperature increases during the growth phase, heat is radiated from the hot smoke layer to unburnt combustible material in the enclosure. Likewise, the heat from the fire radiates to the hot smoke layer, creating an instability in heat flux transfer. The result of this instability is a drastic increase in temperature and heat released from the fire. This transition can be very sudden, with the fire jumping from a seemingly benign state to a fully-developed blaze within a time period of 20-120 seconds [5].

This transition from fire growth to fully-developed burning is known as flashover. This is a phenomenon associated with the thermal instability in the room, and the end result is a rapid increase in temperature, from about 400 to 1200 ℃, as well as a drastic increase in heat flux from the fire, typically from $20\ kW/m^2$ to $150\ kW/m^2$.

There are several definitions of flashover among the literature. Flashover is defined by the International Standards Organization as "the rapid transition to a stage of total surface involvement in a fire of combustible material within an enclosure" [6]. This term is used as the demarcation point between pre-flashover

and post-flashover stages of a compartment fire in fire protection engineering. The Society of Fire Protection Engineers defines flashover as the "point in growth of a flaming fire where the flames are no longer confined to burning items, but also occur within the fire effluent, remote from the seat of the fire" [4]. Among the variations in precise definitions, the important characteristic of flashover is that it is a transition from an environment that firefighters may find tenable while they are fighting the fire, to an extremely hot and dangerous environment that even firefighters cannot survive.

For purposes of the design of the thermoacoustic flashover detector, the criteria for flashover used will be when the smoke layer in the compartment $500 - 600\,°C$ or that the radiation from the hot smoke layer to the floor of the compartment is $15 - 20\,kW/m^2$ [5].

It is very critical that any person inside the burning compartment should exit well before flashover occurs, including firefighters. Even in the turnout gear, the extreme temperatures during flashover will not allow for survival. Furthermore, the structure may become unstable during or after flashover as a result of the fire.

The thermoacoustic flashover detector should emit the tone 1-2 minutes before flashover occurs to allow the firefighter time to exit the enclosure. This is slightly before radiant emissions from the ceiling layer reach $15\,kW/m^2$ or when the ceiling layer temperature reaches $600\,°C$. The device will ultimately be calibrated so that levels slightly below these criteria will produce the warning tone.

The thermoacoustic flashover warning detector will convert the incoming radiant energy from the hot smoke layer into a loud tone without batteries, electricity or moving parts. This is particularly important as it makes the device more robust and eliminates the need for recharging or changing batteries. Not having moving parts increases the longevity of the device by reducing the probability that a part will fail.

This thesis will introduce the concept of thermoacoustics and the parameters necessary for functioning of the device. The prototype of the device will be presented and different materials and dimensions will be analyzed. For the dimensions under consideration, the necessary power input and temperatures will be determined.

1.2. Thermoacoustics Overview

The phenomenon of thermoacoustics operates off the expansion and compression of gas within a cavity to produce an oscillation that results in an audible sound wave.

Thermoacoustic devices consist of two categories: engines and refrigerators. Thermoacoustic engines convert heat to work or acoustic power, and are also termed "prime movers." Thermoacoustic refrigerators convert acoustic power to cooling power and are also termed "heat pumps"[7]. Both types operate on the principles of thermodynamics as shown below in Figure 1-2. Engines require energy input, $\dot{Q}_H$, from a heat source at T_H. Energy is rejected at a rate $\dot{Q}_0$ at a lower temperature, T_o and work is produced at a rate $\dot{W}$ as output. Refrigerators require work as an input, and provide heat as an output. This project

concerns a device converting heat into acoustic power, and therefore the focus of this overview will remain on thermoacoustic engines.
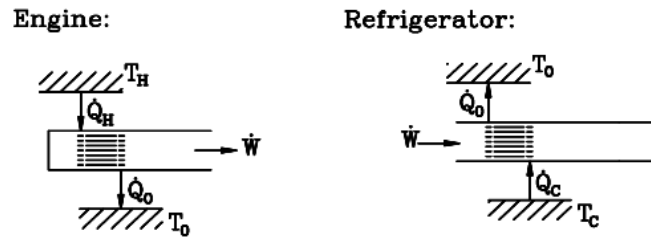
Figure 1-2. Simplified diagram of an engine and refrigerator [8].

There are currently three types of varieties of thermoacoustic engines in the literature: standing-wave engines, traveling wave engines, and pulse combustors [7]. Standing wave engines are called such because the time phasing between pressure and velocity is close to 90°, that of a standing sinusoidal wave. If it were exactly that of a standing wave, the power would be zero at all x-locations, so in reality the phasing is slightly smaller or larger than 90° by a few degrees, typically within $\pm 5^o$. Traveling wave engines are similar, but the time phasing of the pressure and velocity travels from left to right during the oscillation for a rightward moving wave [7].

Traveling-wave engines and pulse combustors are more complex to design than standing-wave engines, are typically larger, and require more components. They are often used for energy functions such as energy harvesting. These functions are not necessary for the thermoacoustic flashover detector, in which the primary output is solely the sound. Therefore the standing-wave engine will be described in further detail. It is rather simple to design for small devices, and operates primarily on a temperature gradient imposed in the device and power

6

input. These are a function of the material properties and the geometry of the device [9].

Standing-wave thermoacoustic engines operate within a resonator of length L, which is a tube (usually with a constant inside cross-sectional area) with one closed end and one open end as shown in Figure 1-3.
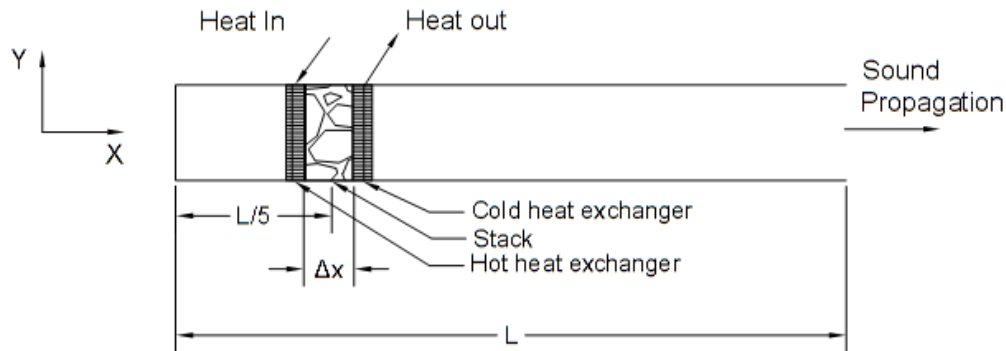
Figure 1-3. Schematic of a standing-wave thermoacoustic engine.

A porous stack of length Δx is positioned in the left side of the resonator near the closed end as shown above. Heat exchangers are positioned on each side of the stack to supply and remove heat to and from the stack. A hot heat exchanger is located on the left side nearest to the closed end, and a cold heat exchanger is located on the right side of the stack. The cold heat exchanger is often termed an ambient heat exchanger, as this side may or may not be actively cooled, and may simply be open to the ambient environment with no cold heat exchanger at all.

The driving power originates from the heat input to the hot heat exchanger, causing an axial temperature gradient along the stack length in the x-direction. The heat input and temperature gradient are necessary parameters

resulting in sound propagation in the positive x-direction. There is an onset level temperature gradient and power input that initiates the oscillation. Below this level, the oscillation either does not occur or dies away. These oscillations are sustained by the heat input to the stack causing the temperature gradient [10].

1.2.1. Thermoacoustic Mechanisms

Thermoacoustic devices operate through the excitement of gas parcels, which are small groups of gas molecules that move together. Each gas parcel interacts with other gas parcels, with each parcel undergoing a thermodynamic cycle which together contributes to oscillations of pressure, velocity and temperature as functions of both space (x) and time (t). This is achieved by the power input imposing a temperature gradient across the stack.

Consider a gas parcel between two heated parallel plates as shown in Figure 1-4. The parallel plates represent magnified portions of the stack through which heat transfer occurs between the solid stack and gas. The hot end will be the left side of the stack, and the cool end will be the right side of the stack.

In the hot portion of the stack, the solid temperature is hotter than the gas parcel temperature, so heat is transferred from the stack to the gas. As the gas parcel heats up, the temperature and pressure increase. This causes the gas parcel to expand, pushing it to a cooler area to the right, where there is lower pressure. Here, the gas parcel is hotter than the adjacent stack, so the gas parcel transfers heat to the stack. As the gas parcel cools it contracts, causing a pressure vacuum which forces the gas back to the left, hotter region. Back at the original position, the process is repeated [8].
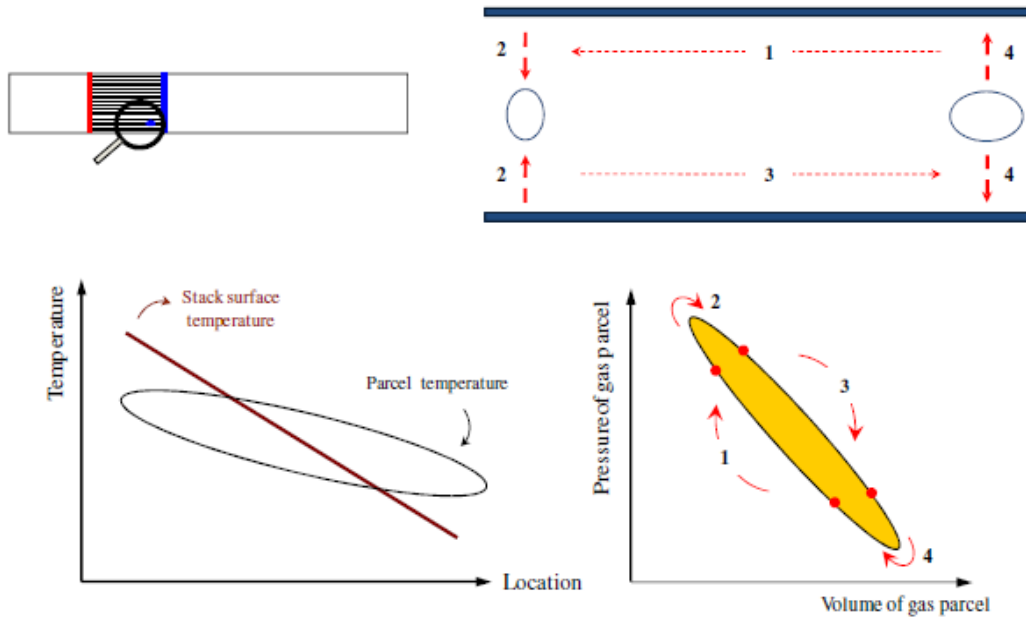
Figure 1-4. Processes within a standing wave thermoacoustic engine [30].

Because the thermal expansion occurs at a higher pressure than its thermal contraction, $\oint p\,dV > 0$ and the pressure-volume ellipse circulates clockwise. This indicates that the gas does work on its surroundings and acoustic power is produced [11].

As this cycle occurs for all the gas parcels in the stack, there is a cumulative effect. This cumulative effect of each gas parcel passing heat to the adjacent cooler parcels in parallel within the stack produces the total acoustic power of the overall process within the acoustic cavity [12]. The length of the stack is larger than the gas displacement of a single gas parcel, so heat transfer occurs along the parcels similar to a bucket brigade as shown in Figure 1-5.

This figure illustrates the overall temperature gradient in the stack, and the heat transfer between the plates of the stack and the gas. Each gas parcel is oscillating in both space and temperature. During this cycle of expansion and

9
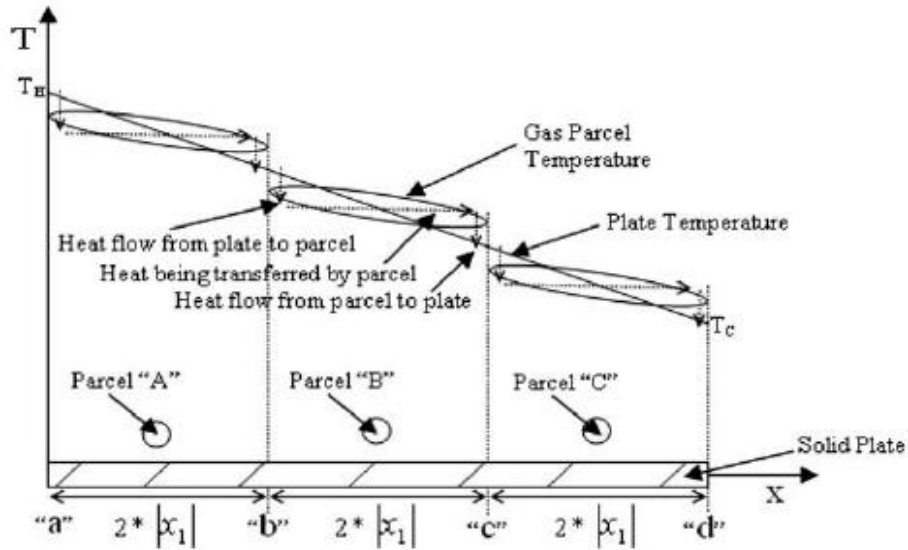
Figure 1-5. Mechanism of heat transfer by the gas parcels along the stack plate [11].

compression, the gas parcel oscillates back and forth along the x-direction as it interacts with adjacent plates. The amplitude of this oscillation is termed the gas displacement amplitude, $|x_1|$, and the total distance that the parcel covers in its movement back and forth is $2|x_1|$ [11].

It is important to note that the gas parcel temperature does not exactly match the stack surface temperature. The stack surface temperature is a linear function of x, imposed by the temperature difference between the hot and cold heat exchangers. Close to the hot heat exchanger, the gas parcel temperature is lower than that of the stack surface, and heat transfer occurs from the stack to the gas parcel. Close to the cold heat exchanger, the gas parcel temperature is higher than that of the stack surface, and heat is transferred from the gas parcel to the stack.

Likewise, the pressure and temperature are oscillating with amplitudes of $|p_1|$ and $|T_1|$ respectively. These are each functions of both space (x) and time (t).

The pressure as a function of space and time is shown as follows [7]:

$$p(x,t) = p_m + Re[p_1(x)e^{i\omega t}] \tag{1-1}$$

By the boundary layer approximation, the spacing between the plates of the stack, y_0, is $\delta_K \leq y_0 \leq 2\delta_K$. The short stack approximation assumes that the length of the stack is considered to be significantly less than that of the wavelength such that it does not perturb the acoustic standing wave. Approximating standing wave phasing between pressure and velocity, the velocity and pressure amplitudes can be expressed as [11]:

$$p_1 = P_A \cos(kx) \tag{1-2}$$

$$u_1 = \left(1 + \frac{l}{y_0}\right)\left(\frac{P_A}{\rho_m a}\right)\sin(kx) \tag{1-3}$$

Where here, $k = spring\ constant\ of\ gas$.

At any given point in time, both the pressure and velocity may be plotted as a function of length along the tube. At x=0 (closed end), the pressure is at a maximum (antinode) and velocity is zero. At x=L, at the open end of the tube, the velocity is at a maximum amplitude and pressure is zero. These are characteristic of a quarter-wavelength standing-wave resonator, with one closed end and one open end.

If one particular point in space were to be plotted as a function of time, the pressure would oscillate between the maximum amplitude as plotted in the pressure vs. length plot. The same is true for the plot of velocity vs. time.

In a thermoacoustic device, time phasing plays an important role. To attain the proper phasing, it is desirable to have poor thermal contact between the gas

parcel and the adjacent surface of the stack. Therefore the gaps between each surface of the stack should be on the order of twice the thermal penetration depth [11]. This causes the heat flow between the gas and stack rather than producing instantaneous changes in gas temperature. This heat flow creates a time phasing between temperature, pressure and displacement that drives the gas particles through the thermodynamic cycle [11].

In the design of a thermoacoustic device, it is important to consider length scales, as the geometry has an effect on the requirements for operation of the device. Some important length scales that will be presented include the sound wavelength, gas displacement amplitude, and viscous and thermal penetration depths. The first two are important along the direction of sound wave propagation, which is denoted as the x-direction. The viscous and thermal penetration depths are important in the direction perpendicular to the direction of sound wave propagation, which is denoted as the y-direction.

The wavelength of sound is important along the x-direction of the sound wave propagation, which is the direction of gas motion. The wavelength of sound, λ, is [8]:

$$\lambda = \frac{a}{f} \tag{1-4}$$

The speed of sound here is a function of gas temperature:

$$a = \sqrt{\gamma R T_m} \tag{1-5}$$

Where:
$\gamma = 1.4 \; for \; air$
$R = 287 \frac{kJ}{kg} for \; air$
$T_m = \frac{T_{hot} + T_{cold}}{2}$

It can be observed that by substituting $T = 293\ K$, the corresponding speed of sound is $a = 343\ m/s$. This is in agreement with the speed of sound at room temperature. With an increase in temperature, the speed of sound increases as well. In the thermoacoustic resonator, the speed of sound will be calculated by using the mean temperature across the stack, which will be simplified as the average temperature of the hot and cold heat exchangers.

In a standing-wave engine consisting of a resonator with one closed and one open end, the resonator length is a quarter of the total wavelength of the sound produced [8]. Denoting the resonator length as L, the wavelength can also be expressed as:

$$\lambda = 4L \tag{1-6}$$

The angular frequency, ω, can be related to the frequency by the following equation:

$$\omega = 2\pi f \tag{1-7}$$

Combining Equations 1-4 and 1-8, an expression can be derived linking the angular frequency to the length of the resonator:

$$\omega = \frac{a\pi}{2L} \tag{1-8}$$

It can then be seen that for a given working gas, the angular frequency of the sound wave is a function of the mean gas temperature T_m and the resonator length L:

$$\omega = \frac{\pi\sqrt{\gamma R T_m}}{2L} \tag{1-9}$$

This equation shows that for a constant mean temperature, a decrease in resonator length corresponds with an increase in frequency. This was confirmed in experiments by Jung and Matveev [13].

The angular frequency will be used in further equations. In calculating the speed of sound based on the gas temperature, and then calculating the frequency of the sound wave, the above equations show reasonable agreement within the range of measured values. Slight inaccuracies may result from different temperatures, but the equations give a good estimation of the frequency. In the case of standing-wave thermoacoustic engines, the gas inertia contributes to the resonance behavior because there are no mechanical moving parts within the system. The lengths of the heat-exchange components are much shorter than the wavelength [8].

The gas displacement amplitude, $|x_1|$, is also an important length scale in the direction of the gas motion. This is represented as an absolute value because the gas is oscillating around its original location, and the amplitude of the oscillation is of interest[8]:

$$|x_1| = \frac{|U_1|}{\omega} \tag{1-10}$$

The gas displacement amplitude is often a very large fraction of the stack length and may be larger than the lengths of the heat exchangers (8). This displacement is always shorter than the wavelength.

Perpendicular to the gas motion, the two important characteristic lengths are the thermal penetration depth, δ_κ, and the viscous penetration depth, δ_υ. These are defined by [8]:

$$\delta_\kappa = \sqrt{2k/\omega\rho c_p} = \sqrt{2\kappa/\omega} \tag{1-11}$$

$$\delta_\upsilon = \sqrt{2\mu/\omega\rho} = \sqrt{2\upsilon/\omega} \tag{1-12}$$

The variables above are all properties of the gas within the resonator, which is air initially at standard temperature and pressure. These two characteristic lengths describe how far heat and momentum can diffuse laterally during a time interval of the order of the period of the oscillation divided by π. At distances much greater than δ_κ and δ_υ from the solid boundary, the gas feels no thermal contact or viscous contact with the solid boundaries. The heat exchange components must have lateral dimensions of the order of δ_κ in order to exchange heat with the working gas. The gaps in the stack should have dimensions on the order of $2\delta_\kappa$ to provide imperfect heating to the gas [8].

If the ratio of the square of these two penetration depths is taken, the Prandtl number, σ, is obtained [8]:

$$\left(\frac{\delta_\upsilon}{\delta_\kappa}\right)^2 = \frac{\mu c_p}{k} = \sigma \leq\sim 1 \tag{1-13}$$

Because the Prandtl number is close to unity, this shows that the viscous and thermal penetration depths are comparable. Therefore thermoacoustic engines typically suffer from substantial viscous effects [8].

A summary of the hierarchy of the length scales is as follows [8]:

$$\delta_\upsilon, \delta_\kappa \ll |x_1| \ll \lambda$$

It is interesting to estimate the thermal and viscous boundary layers within a thermoacoustic engine. As the temperature of the gas increases, the boundary layers increase slightly. For example, the boundary layers for a sound wave with a frequency of $f = 500\ Hz$ and corresponding $\omega = 3142\ rad/s$ can be calculated

15

using the following gas properties at the temperatures of ambient air at 20 ℃ and heated air at 227 ℃:

Air Properties [14]	20 ℃	227 ℃
$k \, (kW/m℃)$	$2.624 * 10^{-5}$	$4.04 * 10^{-5}$
$\rho \, (kg/m^3)$	1.177	0.706
$\mu \, (kg/ms)$	$1.846 * 10^{-5}$	$2.67 * 10^{-5}$
$c_p(kJ/kgK)$	1.0049	1.0295

Table 1-1. Air properties at selected temperatures.

This gives the following thermal and viscous boundary layer depths at each temperature:

Boundary Layer	20 ℃	227 ℃
$\delta_\kappa(mm)$	0.1188	0.1882
$\delta_v \, (mm)$	0.0999	0.1552

Table 1-2. Boundary layer depths at selected temperatures.

With these calculations, the Prandtl number was also calculated as a check. At 20 ℃, the calculated value was 0.707, while the tabulated value was 0.713. At 227 ℃, the calculated value was 0.68, while the tabulated value was 0.68. This confirms the validity of the correlation for the boundary layers.

In this example, the thermal boundary layer, δ_κ, ranges from about 0.12 mm to 0.19 mm as the temperature increases in the range evaluated. The viscous boundary layer, δ_v, increases from about 0.10 mm to 0.16 mm. This shows that there is not a constant boundary layer throughout the thermoacoustic engine because there are different gas temperatures within the resonator in the hot and cold portions of the device. The distance between the solid components within the stack should be about 0.4 mm.

In the example, the wavelength would be 0.686 m, so a quarter-wavelength resonator would have a length on the order of 17 cm. Assuming that the ratio of resonator length-to-diameter is about 8, the corresponding diameter of the resonator would be 2 cm. This shows that the boundary layer depths of 0.10 to 0.20 mm are extremely small compared to overall dimensions of the thermoacoustic engine.

The thermal and viscous penetration depths are important to consider because they indicate the thickness of air above and beneath each heated section of the stack beyond which thermal conduction and viscous effects are negligible. For a parallel-plate stack design, the distance between plates should be about $2\delta_K$.

The critical temperature gradient marks the point at which no temperature oscillations will occur. If the temperature gradient is below the critical value, the device is a refrigerator. If the temperature gradient is above the critical value, the device is an engine and converts heat to sound [9]. Therefore in this design, the temperature gradient across the stack should be larger than the critical temperature gradient for the device to produce sound.

The critical temperature gradient from Equation 4.44 of *Thermoacoustics: a Unifying Perspective* by Swift is reproduced below [8]:

$$\nabla T_{crit} = \frac{\omega A |p_1|}{\rho_m c_p |U_1|} \tag{1-14}$$

This suggests that all other variables held constant, a smaller cross-sectional area of the resonator will require a lower temperature gradient for sound. This concept agrees with the trend by which Symko was able to produce sound with a temperature difference of 40 ℃ in a 2-cm long resonator [15]. This

temperature difference is much lower than the temperature difference of ~213 ℃ required by Jung and Matveev in a 10-cm long resonator with a 14 mm diameter cross-section [13].

This critical temperature gradient may be compared to the actual temperature gradient across the stack. With the hot heat exchanger and the cold or ambient heat exchanger on either side of the stack, there is a temperature gradient across the stack in the x-direction. This temperature gradient can be calculated by dividing the temperature different across the stack by the length of the stack:

$$\nabla T = \frac{T_{hot} - T_{cold}}{\Delta x} \tag{1-15}$$

1.2.2. Components of Resonator

A standing-wave thermoacoustic engine consists of a tube with one closed end and one open end, termed a resonator. Within this resonator is a short porous stack which provides heat capacity for the gas. Adjacent to each end of the stack is a hot heat exchanger on the side nearest to the closed end of the resonator, and a cold or ambient heat exchanger on the side closest to the open end.

The resonator is simply a tube which is open on one end and closed on the other. This tube contains the heat exchangers and stack [9]. It is completely airtight, with the only opening being the open end of the resonator. The length of the resonator, *L,* is ¼ of the sound wavelength. The interior of the resonator should be a relatively hard material that does not absorb much of the acoustic oscillations so that a sound wave may be audible.

A stack, which consists of a porous material with a high heat capacity, is positioned in the cross-section at a point typically 1/5th to 1/3rd of the resonator

length from the closed end. The ideal position is selected to supply heat to the oscillating gas parcels at the moment of their compression and to remove heat at the moment of their rarefaction [13]. Therefore the stack location should be about $\lambda/20$ from the nearest pressure antinode of the standing wave, which is located at the closed end [8]. Keeping in mind that the resonator length is $1/4^{\text{th}}$ of the wavelength, this implies that the stack center should be positioned at a point near $x_{stack} = \frac{L}{5}$.

The stack provides a heat capacity for the gas while minimizing conduction along the temperature gradient between heat exchangers [8]. It also provides acoustic impedance for the air [16]. An ideal stack has the smallest possible thermal conductance and has hydraulic radii on the order of the thermal boundary layer, $\delta_\kappa \approx 0.1 \; mm$. The gap between the inside wall of the resonator and stack should be no larger than the hydraulic radius of the stack [8].

Some stack configurations in the literature consist of a stainless steel spiral, with the gaps between the layers of the spiral forming parallel-sided thermoacoustic channels. These allow the designer to specify the spacing between plates and input geometric configurations easily into computer models. However, these are very intricate to make and typically require spacers between the spiral layers [8]. This has been done in a thermoacoustic refrigerator by Chinn at the University of Maryland [17].

Another configuration similar to parallel-plate spirals is obtained by stacking flat fiberglass sheets with nylon spacers, held together with epoxy. This was used in the thermoacoustic resonator documented in Wheatley et al. [18].

Manufactured metal, ceramic or plastic honeycomb can also be used for the stack as alternate designs [8].

The simplest, most easily accessible and machinable material for a stack is steel wool, which is currently used in the Pyrex tube thermoacoustic resonator by Baz et al. at the University of Maryland. It is the quickest to make and allows for variation in the porosity of the stack. However, it is a random configuration and is more difficult to attempt to model using software such as DeltaE.

A heat exchanger is positioned on either side of the stack, such that heat is supplied to the stack on the end nearest to the closed end of the resonator, and heat is removed from the stack on the end nearest to the open end of the resonator. The heat exchangers must have a large percentage of open area to allow for movement of the gas parcels. Ideally they should provide good thermal contact with the gas while causing minimal pressure drop [8].

Figure 1-6. Electric-resistance hot heat exchanger used at Los Alamos [8].

The heat exchangers used in a small-scale thermoacoustic design studied by Jung and Matveev include 2 layers of copper screen/mesh in the cross-sectional area of the tube [13].

Some larger designs of heat exchangers used in larger thermoacoustic engines by Greg Swift at Los Alamos
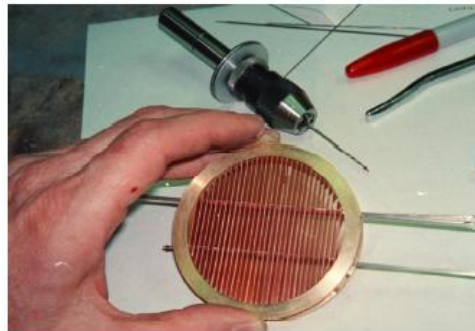
Figure 1-7. Water-cooled ambient-temperature heat exchanger used at Los Alamos [8].

Laboratories include finned-tube and shell-and-tube heat exchangers. The electric resistance hot heat exchanger in Figure 1-6 consists of ceramic "combs" to maintain the spacing between a 6 mm wide, 25 μm thick ribbon of NiCr winding. The water-cooled ambient heat exchanger in Figure 1-7 consists of copper fins extending 13 mm along the length x, into the page. The cold heat exchanger is typically cooled with water tubes or a cooling jacket. For comparison of dimensions, the overall diameter of this resonator is 6.3 cm [8].

1.2.3. Examples

Four examples will be presented to provide insight and a starting point for the design of a small-scale thermoacoustic engine. Jung and Matveev (2009) experimented with a 10 cm long resonator using external heating from a band heater. Symko and McLaughlin (2004) developed 2 cm long resonators using very little power input and temperature differences across the stack. Wheatley et al. (1985) experimented with 30 cm long resonator by establishing a temperature gradient across the stack by putting one end in liquid nitrogen. Baz et al. (2012) produce sound from a 17.5 cm long resonator using an internal resistance wire as a power input. These successful thermoacoustic devices provide examples of possible materials and dimensions for the thermoacoustic flashover detector.

Jung and Matveev (2009) developed and tested a small thermoacoustic engine while varying the overall length. Their work gives a useful comparison of the critical temperature differences associated with different stack positions. The experimental setup was also very detailed and provided insight into materials that can withstand high temperatures and provide adequate air sealing.

The closed end of the device consisted of a flanged copper cap, 15 mm long and with an inner diameter of 14 mm. The stack holder was a 7 mm long piece of ceramic tube with low heat conductivity. The open end consisted of an open copper tube with a flange on one end. Four different lengths of this tube were tested so that the overall length of the variants was 57, 67, 100 and 124 mm. The two flanges were bolted together with the ceramic stack holder in the middle. Graphite gaskets provided airtight seals for the junctions. A schematic and photo of their device is shown in Figure 1-8. The pressure transducer shown was used for measurements and did not provide energy input [13].

The heat exchangers consisted of 2 layers each of 30 x 30 –size copper mesh with wire diameter 0.3 mm. The stack consisted of reticulated vitreous carbon (RVC), which is random porous, open-cell foam similar to a fine metal wool. This RVC was 80 pores-per-inch and was from ERG Materials and Aerospace Corporation. The ratio of pore size to thermal penetration depth was in the range of 2.4, for the engine length of 124 mm, to 3.4, for the engine length of 57 mm.
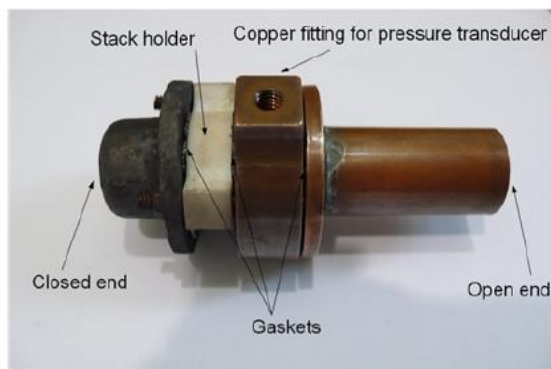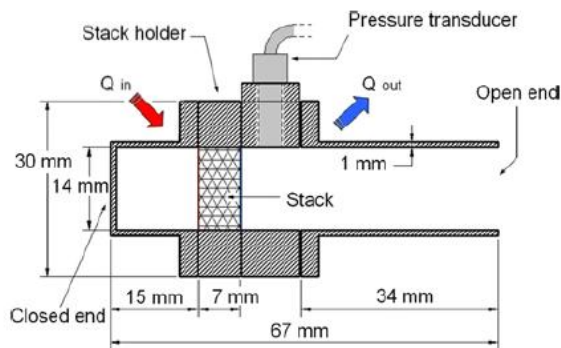
Figure 1-8. Thermoacoustic resonator by Jung and Matveev [13].

22

Heat was input into the hot end using a band heater at a slow heatup rate, resulting in a stack temperature increase of about $2\,°C/min$. The cold end was cooled using a cooling jacket with flowing water[13].

The average temperatures between the hot and cold heat exchangers (mean temperatures) at the onset of sound were in the range of $140 - 190\,°C$. The critical temperature difference including uncertainty ranged from $210 - 308\,°C$ for the varying lengths. The stack length was constant at $\Delta x_{stack} = 7$ mm and the distance of the stack from the closed (left) end was constant at $\Delta x_{stack} = 17.5$ mm for all the test variations [13]. This allows for a comparison of critical temperature difference as a function of stack location and length with respect to the overall device length. The lowest ΔT_{crit} was measured in the device where $\frac{x_{stack}}{L} = 0.18$ and $\frac{\Delta x_{stack}}{L} = 0.07$.

Matveev and Jung noted that the change in stack position with respect to the standing-wave form was one of the factors causing the decrease in critical temperature difference in the 100-mm engine. Other factors contributing to the decrease include an increase in thermal penetration depth and a reduction in losses [13]. The data also shows that shorter resonators correspond with higher frequencies.

Orest Symko and co-workers at the University of Utah have conducted research to convert heat into sound on a very small scale by optimizing the geometry and insulation of the resonator. These devices were on the order of a 2-3 cm long and the stack consisted of random porous material such as cotton wool or glass wool which was evenly dispersed and in thermal contact with the copper

mesh heat exchangers at either end [15]. A device developed by Bonnie McLaughlin had a length of 38 mm and a width of 13 mm, producing sound at $\Delta T = 32\,°C$ across the hot and cold heat exchangers [19]. The sound was produced at ∼2 kHz with an intensity of $10\,mW/cm^2$ from a power input of 2 W. Another student showed that by increasing air pressure, a smaller temperature difference was needed across the heat exchangers to produce sound. This is being developed for microcircuit applications, therefore the temperature difference was established by thermally anchoring the hot heat exchanger to a microelectronics circuit and maintaining the cold heat exchanger at room temperature. Further developments have reduced the threshold temperature difference for oscillations across the stack down to 25 °C [15].

The resonator developed by Wheatley, Hofler, Swift, and Migliori created a tone of 200 Hz by cooling the cold end of a resonator in liquid nitrogen while maintaining the "hot" end at an ambient temperature.

The resonator was 29.5 cm long, consisting of a closed-end copper tube 13.1 cm long and a 14.4 cm long open-open copper tube, connected by the 2 cm long stack holder assembly in the middle. The copper tube had an outer diameter of 3.5 cm and an inner diameter of 3.24 cm. The stack holder was made of poorly conducting stainless steel and was secured between the copper tubes with brass flanges. A schematic of the device is reproduced in Figure 1-9 [18]. In the figure, the central section was a 34.9 mm OD stainless steel tube connected to each copper tube using flanges. Section A-A shows the copper strips used for the heat

exchanger, adhered using a low-melting point solder. Section B-B indicates how the fiberglass plates are packed uniformly within the stainless steel tube.

The stack was made of 22 G-10 fiberglass plates, each 0.38 mm wide and spaced 1 mm apart. These were fit into the inner diameter of the stainless steel tube, which was 16.5 mm in inner diameter. The stainless steel stack holder acted as a thermal insulator. Copper strips were attached to the brass flanges at both ends of the stack to serve as heat exchangers. The flanges were sealed to the copper tubes by a heat sink compound [18].

To operate the device, the open end of the device was immersed in liquid nitrogen, with the liquid level near the flange. The closed end was kept warm with the experimenter's hands. Once the tube was sufficiently cold, it was observed to vibrate at low frequencies. At this point, it was removed from the liquid nitrogen and produced a loud tone at a frequency of 200 Hz [18].

Although the temperature gradient in this device was produced by cooling
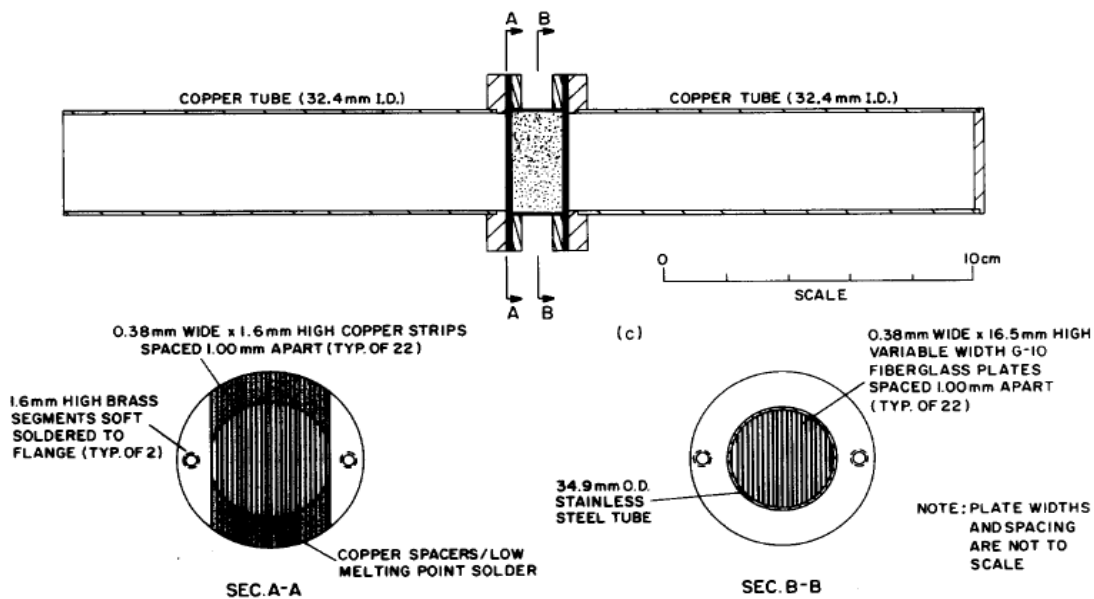
Figure 1-9. Thermoacoustic engine experimented with by Wheatley et al. [18].

the cold end, rather than heating the hot end, it illustrates the importance of the temperature gradient and provides an example of the type of materials that could be used in the device.

The temperature difference across the stack can be estimated because one end was in liquid nitrogen and the other was at ambient, which will be assumed to be $20\,°C$. Liquid nitrogen boils at $-196\,°C$ [20]. Therefore the temperature difference across the stack was $\Delta T \approx 216\,°C$. With the stack length of 2 cm, the temperature gradient across the stack was $\nabla T \approx 108\,°C/cm$.

The initial device and dimensions for the prototype design of the thermoacoustic flashover detector were based on a Pyrex tube resonator developed for energy harvesting research by Baz, Smoker and Nouh at the University of Maryland, College Park [21]. The resonator is a glass Pyrex test tube, with $L = 175\,mm$ and $ID = 20\,mm$. A resistance wire zig-zagging across the cross-section inside the tube provides heat input to the stack at $x = 64\,mm$. This is connected to a direct current power supply. The stack may be easily removed and interchanged because there is no cold heat exchanger.

With a stack size of $\Delta x_{stack} = 2.54\,cm$, a 500 Hz tone is produced upon a power input of 33 W. The sound level measured at 38 mm from the opening along the x-axis is 114 dB with a power input of 33 W, and 122 dB at a power input of 41 W.

1.3. Design Considerations

Ultimately, the thermoacoustic flashover detector is planned to operate without electricity by using only the radiant heat from the hot gas layer in a

compartment fire. For the prototype design, this heat is simulated using a heater located outside of the resonator.

The design originated with the Pyrex test tube resonator because this was a working design which was accessible in-house at the University of Maryland. The primary constraint of the thermoacoustic flashover detector was that it needed to be based on heat input from the outside and therefore the resistance wire needed to be replaced with a different heat exchanger which could be powered from the radiant heat from the hot gas layer in an impending flashover scenario.

There is a critical power input and temperature gradient across the stack necessary to produce sound. Because the applied temperature gradient is simply $\nabla T = \Delta T / \Delta x$, a shorter stack length corresponds to a steeper temperature gradient given a constant temperature difference. Therefore a shorter stack would require a lower power input and smaller temperature difference to produce the same temperature gradient as a longer stack. This was confirmed in tests using the Pyrex tube resonator.

Shorter resonators correspond with higher frequencies, while longer resonators correspond with lower frequencies. This is due to the larger surface area for energy dissipation in longer resonators [13]. For example, a 2 cm long resonator produced a frequency of 2 kHz, while a 6.7 cm long resonator by Jung and Matveev produced a 1.7 kHz frequency. The 12.4 cm long engine by Jung and Matveev produced an even lower frequency at 940 Hz [13, 22], while the 17.5 cm Pyrex tube resonator produced a frequency of 500 Hz.

Based on experimental work, the resonator should be shaped having a length to inner diameter ratio of approximately 8 to 50, with $\frac{L}{D} = 12$ giving the best results [16]. For comparison, the Pyrex tube resonator has $\frac{L}{D} = 8.75$ and performed well.

For an acoustic sound to be generated, it is mandatory that the resonator be airtight. Even the tiniest leak from the system will prevent the gas parcels from oscillating in a manner to produce a sound wave. It is therefore mandatory that the only open portion of the resonator is the open end through which the sound wave propagates [13].

The critical minimum heat input, minimum temperature difference across the stack and mean operating temperature will be evaluated for the prototype of the thermoacoustic flashover detector. These are expected to be a function of the device geometry, materials and stack location within the resonator [9].

2. Experimental Setup

The prototype of the thermoacoustic flashover detector contains five separate sections that are held together via compression to form an airtight resonator. This was accomplished by using a threaded pipe nipple for the open end of the resonator and joining the open end to a matching flange. At the other end of the resonator, the ceramic closed end was pushed against an aluminum flange cap, with three layers of thin rubber between the ceramic and flange cap to prevent cracking of the ceramic cap when compressed. The heat exchangers and ceramic stack holder were stacked in succession, with graphite gaskets forming a seal between the copper and ceramic at junctions as shown in Figure 2-1.

The entire assembly was bolted together with rods through the flange holes to form the device. Changing the orientation of the device did not prevent sound from occurring, and the simplest setup to allow for visible, even
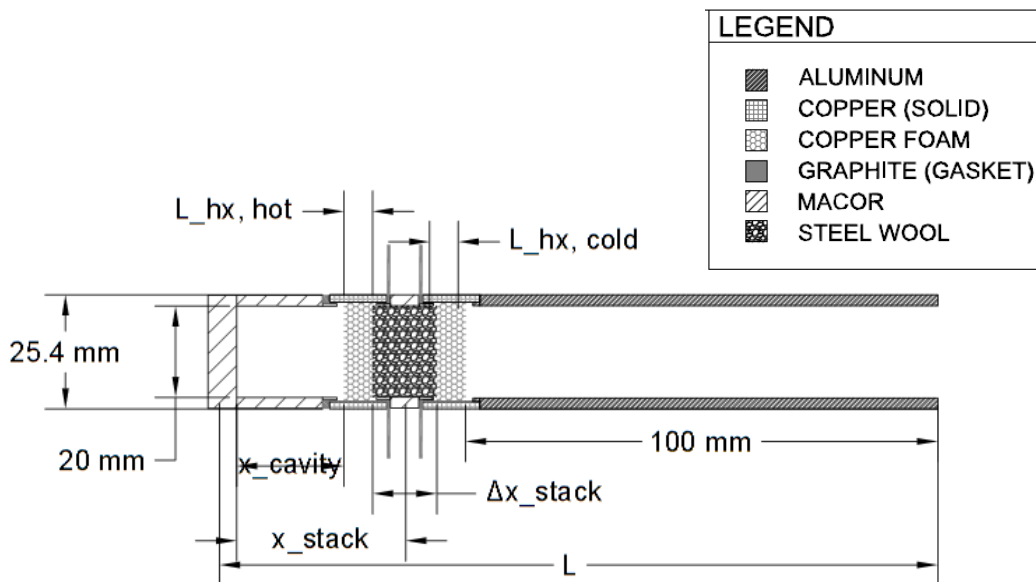
Figure 2-1. Schematic of thermoacoustic flashover detector.

compression of the device was in the upright position. The band heater was wrapped around the heat exchanger to the left of the stack. The cooling ice/water bath was around the heat exchanger to the right of the stack. A photo of the full assembly is shown in Figure 2-2 with the band heater and cooling section.

Two designs with different lengths were built and tested. Design #1 consisted of a longer stack, hot heat exchanger, and cap. This design was the first to be repeatable, but further research pointed to a shorter stack and cap as requiring lower temperatures for sound onset. Therefore Design #2 was built for comparison. A summary of the dimensions is provided in Table 2-1.

Inner Lengths (mm)	Design #1	Design #2
Cap cavity	38.1	19.05
$L_{hx,hot}$	12.7	6.35
Δx_{stack}	20.32	12.7
$L_{hx,cold}$	6.35	6.35
Aluminum end	101.6	101.6
Gaskets	3.175	3.175
L	183	150
x_{stack}	62.5	33.3

Table 2-1. Lengths of components in each design.

Figure 2-2. Prototype design of thermoacoustic flashover detector.

Design #1 includes a stack with length $\Delta x_{stack} = 20\ mm$ positioned at a point within the resonator where the stack center corresponds with $\frac{x_{stack}}{L} \approx 0.33$. Design #2 includes a stack with length $\Delta x_{stack} = 15\ mm$ positioned at a point within the resonator where the stack center corresponds with $\frac{x_{stack}}{L} \approx 0.20$. The second design is shorter than the first,

and was built to compare the effect of different dimensions on the critical temperatures at sound onset.

A 25.4 mm band heater was used as the heat source (Chromalox MB1A1A1A1 from Omega). This heater had an inner diameter of 25.4 mm and a band width of 25.4 mm. The power of the heater was 100 W; the power density of the heater surface was $0.0496 \, W/mm^2$ [23]. This heater fit snugly around the copper ring heat of the exchanger. However, the heater was longer than the heat exchanger and hung over the ceramic portion as well. Also, the heater was one piece and needed to be slipped around the device during assembly, before wider parts were added above it.

2.1. Device Assembly

The design for the resonator included two heat exchangers and three separate pieces for the resonator sections: a cap, stack holder, and open tube. The cap and stack holder were both Macor machinable ceramic. The open tube was an aluminum pipe nipple connected to a flange for compression of the device. The heat exchangers were each copper rings with copper foam brazed inside to provide good heat transfer from the outside to inside of each heat exchanger. To hold the device together via compression, flanges were bolted together at either end and graphite gaskets were used as seals between the copper and ceramic at junctions.

The heat exchangers consisted of copper rings with copper foam discs brazed to the inside diameter. These parts were manufactured by ERG Aerospace

Corporation and provided excellent heat transfer from the outside of the ring to the inside foam surface.

The copper rings had an outer diameter of 25.4 mm and an inner diameter of 22 mm, corresponding to a wall thickness of 1.65 mm. The copper foam was Duocel copper foam alloy C10100. This is a rigid, highly porous and permeable structure of copper forming a skeletal metal structure which is termed as copper foam. The type of copper foam used had 20 pores per inch (20 PPI) with 8-12% nominal density [24].

Two sizes of heat exchangers were used in experiments: 12.7 mm and 19.05 mm long heat exchangers. The 12.7 mm long heat exchangers consisted of a 6.35 mm thick disc of copper foam centered in the ring, Within the resonator, this corresponded to a heat exchanger length of $L_{hx} = 6.35\ mm$.

The 19.05 mm long pieces contained a 12.7 mm long disc of foam centered in the ring, corresponding to a heat exchanger length of $L_{hx} = 12.7\ mm$.

Each heat exchanger had a 3.175 mm clearance on either side of the copper foam inside the ring. This clearance was to allow the ring to slip over the adjacent piece in the overall design. Photos of the copper foam heat exchangers are
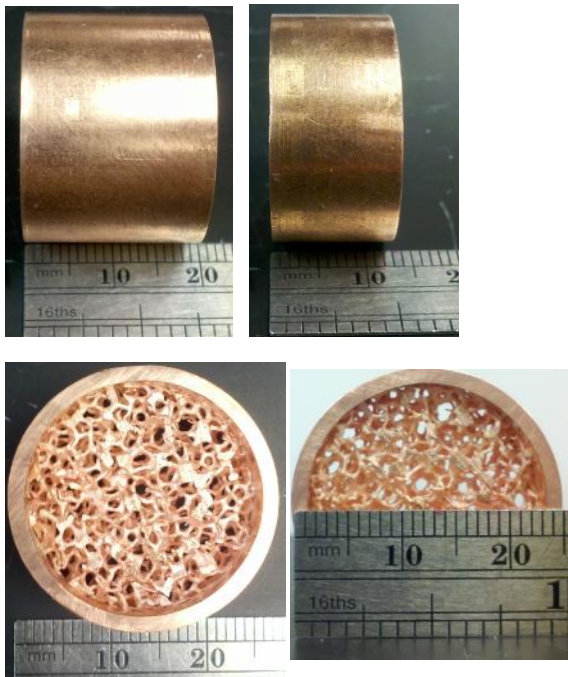

Figure 2-3. Copper foam heat exchangers.

shown in Figure 2-3, showing the longer one on the left and the shorter one on the right with views from the front and the side.

In the device assembly, the cold heat exchanger was the shorter piece. In Design #1, the hot heat exchanger was the longer piece, while in Design #2, the hot heat exchanger was the shorter piece.

Prior to assembling the device, the heat transfer of the heat exchangers was evaluated. This involved heating the outside surface of the copper ring using the 25.4 mm band heater which was used as the heater in the experiments. The heatup rate and temperature difference between the outside copper ring surface and the inner center surface of the foam was measured. It was observed that the temperature across the surface of the copper foam was uniform throughout the volume of the foam.

The tests were done using a variable transformer to evaluate heatup rate differences at 50% power and 100% power. One thermocouple was placed on the surface of the copper foam inside, and the other thermocouple was placed on the outside surface of the copper ring under the band heater. These tests were conducted using the longer heat exchanger (19.05 mm length). The band heater length was 25.4 mm and therefore not all the energy into the heater went directly into the heat exchanger.

First, the power was set to 50% for about two minutes, until the outside copper temperature reached 80℃. Then the power was increased to 100% and run for an additional 2 minutes. The temperature difference between the outside surface of the copper ring and the inside surface of the foam was calculated.

At 50% power, the average temperature difference from the outside to inside was 1.8 ℃. At 100% power, the average temperature difference was 5.3 ℃. Based on these results, it may be assumed that the temperature of the heat exchanger in contact with the stack is within $5\ ℃ - 10\ ℃$ of the outside copper temperature. This simplifies the final diagnostics of measuring the temperature difference across the stack.by allowing the outside copper temperature to be measured with a thermocouple and assuming that the hot heat exchanger temperature is within this range.

The cap and stack holder were machined pieces of 25.4 mm diameter ceramic rods. Ceramic was chosen because it can withstand high temperatures up to 800 ℃ continuously and is more durable than glass [25].

The pieces were designed so that the copper ring of the heat exchangers could be slipped over the ends of the ceramic at junctions, allowing for a gasket to be sandwiched between the copper and ceramic. Design #1 utilized the longer pieces, and Design #2 utilized the shorter pieces. In Design #1, the length of the inside cavity within the end cap was 42.8 mm and the total stack holder length was
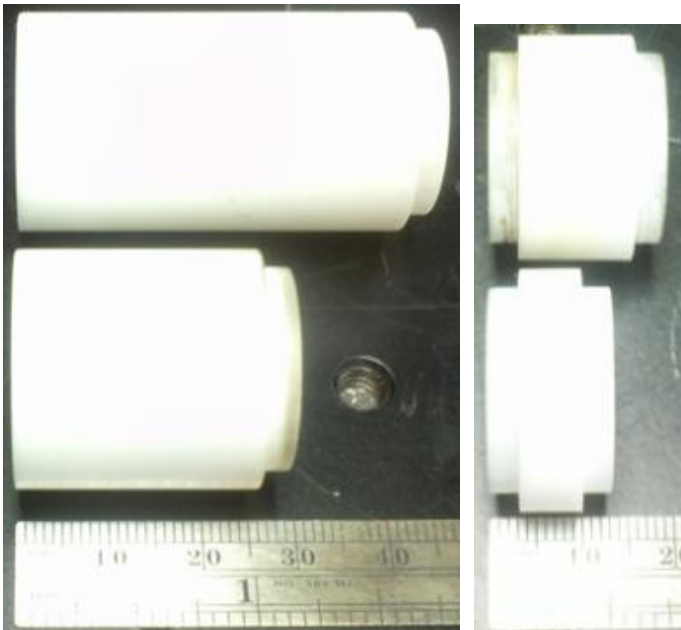
Figure 2-4. Macor ceramic end caps (left) and stack holders (right).

19.05 mm. In Design #2, the length of the cavity within the end cap was 23.8 mm and the total stack holder length was 12.7 mm.

In calculating the stack length, the actual stack length is slightly longer because it was sandwiched between the heat exchangers and was therefore slightly longer than the total stack holder length. A photo of each end cap and stack holder is provided in Figure 2-4.

The open-ended portion of the resonator was a ¼ NPT standard aluminum threaded pipe nipple. The pipe size corresponded to an outer diameter of ~25.5 mm and an inner diameter of ~22 mm. The initial length of the nipple was 127 mm, but on one end the threads were lathed down and the outer diameter was reduced to 22.098 mm for the end length of 1.5875 mm to fit into the adjacent copper piece. This was done for the length on that end so that the pipe would not push against the copper foam within the ring. The other end of the pipe nipple was connected to a threaded flange.

The stack was formed from a small bundle of steel wool that was loosely rolled to fit between the hot and cold heat exchangers such that the density of the stack was $\rho_{stack} \approx 156 \, kg/m^3$. The thickness of each steel fiber is estimated to be 0.08 to 0.11 mm, which is on the order of δ_K.

The steel wool obtained was initially a rolled up pad, about 50 mm by 50 mm. This was partially unrolled, and a strip about 25 mm wide by 100 mm long was cut off as shown in Figure 2-5. This strip was rolled loosely to form a cylinder 20 mm in diameter to fit inside the stack holder.

Figure 2-5. Strip of steel wool cut from initial sample to form the stack.

The length of the stack was the distance between the surfaces of the hot and cold heat exchangers, and therefore was longer for Design #1 and shorter for Design #2. A photo of each stack is shown in Figure 2-6. In the photo, the stack in the top was 20 mm long and was used in Design #1. The stack on the bottom was 15 mm long and was used in Design #2. The discoloration in the top stack was due to heating during use.

During assembly, the stack was placed into the stack holder between the hot and cold heat exchangers. Care was taken to ensure that each end of the stack was in contact with each heat exchanger, and the outside circumference of the stack filled the inside of the stack holder. A photo of the stack within the device prior to addition of the cold heat exchanger is provided in Figure 2-7.

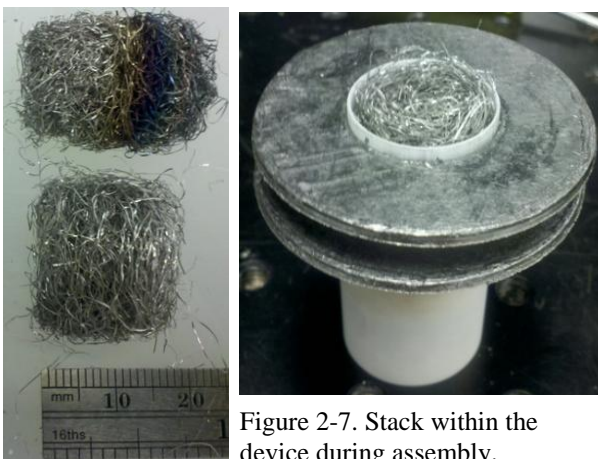Each stack was weighed and the density was calculated. Each stack had almost an identical density as shown in Table 2-2. Stack #1 was used in Design #1, and Stack #2 was used in Design #2. The average stack density was $\rho_{stack} = 156.5 \ kg/m^3$.

Figure 2-6. Close-up of stack.

Figure 2-7. Stack within the device during assembly.

	Δx_{stack}	$Weight_{stack}$	ρ_{stack}
Stack #1	$20\ mm$	$1.02\ g$	$155\ kg/m^3$
Stack #2	$15\ mm$	$0.77\ g$	$158\ kg/m^3$

Table 2-2. Stack length and density for each stack used.

2.1.1. Seals

Using multiple pieces provided a challenge of sealing the resonator so that there were no air leaks. Any air leak prevents the device from producing a sound. The joints between the copper and ceramic were sealed by graphite gaskets under compression via the flanges and bolts. The joint between the cold heat exchanger and aluminum pipe was sealed using sealant. After assembly and prior to operation, the resonator was tested for air leaks via slight interior pressurization and a surfactant formula applied to the outside of the joints.

Graphite gaskets were used for seals between the ceramic and copper pieces. Graphite was chosen because it withstands high temperatures and performed successfully in the resonator tested by Jung and Matveev [13]. It proved to be successful in this design as well.

Two types of gaskets (from McMaster Carr) were initially tried. Each had a thickness of 1.5875 mm, an inner diameter of 21.43 mm and an outer diameter of 47.625 mm. The first type was composed of graphite with a Buna-N binder and could withstand temperatures up to 343 ℃ . The second type was a compressible graphite gasket that could withstand temperatures up to 454 ℃. This had no binder and contained a 0.0508 mm thick stainless steel insert ring to give added strength [26].

The second type proved to give a much better airtight seal at junctions because of its superior compressibility. However, the first type allowed itself to be

cut without falling apart. The gasket between the ceramic cap and hot heat exchanger needed to be trimmed so that the 25.4 mm band heater could fit over the hot heat exchanger, gasket, and portion of the ceramic cap. Therefore the first type was used at this junction, and the second type was used at all other copper/ceramic junctions.

In Figure 2-9, the top left gasket was trimmed so that the outer diameter was 25mm, producing the gasket in the bottom left corner. This fit underneath the band heater, for the junction between the cap and hot heat exchanger. The two right gaskets shown were used on either side of the stack holder.

Figure 2-8. Inside of stack holder during assembly.
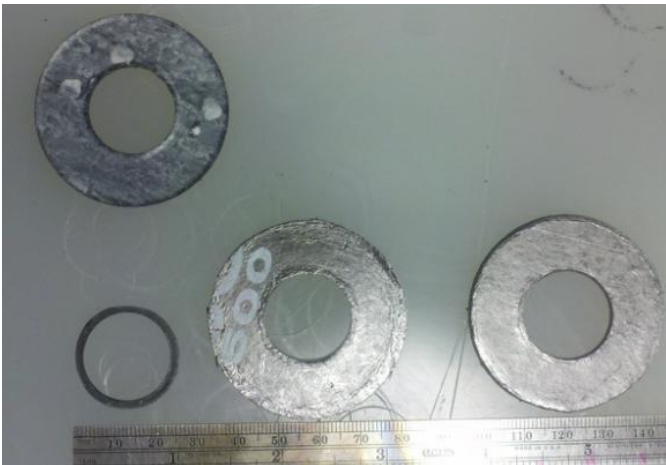
Figure 2-9. Graphite gaskets used in thermoacoustic flashover detector.

A photo of the inside of the stack holder during assembly, prior to the insertion of the stack and heat exchanger connection is provided in Figure 2-8. Post-assembly, the external close-up view of the stack holder and seals are shown in Figure 2-10. In this photo, above and below the ceramic stack holder are the compressible graphite gaskets which separate the ceramic from each copper heat exchanger. A trimmed gasket can be seen between the hot heat exchanger and the bottom ceramic cap piece. Above the top gasket is

38

the cold heat exchanager which is hidden from view by the styrofoam cup. Below the lower gasket is the hot heat exchanger which is partially hidden from view by the 25.4 mm band heater.

The cold heat exchanger was connected to one end of the aluminum pipe nipple using Permatex RTV clear sealant. Prior to connection, the pipe nipple was modified and trimmed slightly so that the threads on one end were eliminated, and the outer

Figure 2-10. Close-up of stack holder post-assembly

diameter was trimmed with a lathe so that it was slightly smaller than the inner diameter of the copper ring of the heat exchanger. This was done for a length of ~1.5875 mm on the end so that the aluminum would not push against the copper foam, which was inside the copper ring with a clearance of ~3.175 mm from each end. The other end of the pipe nipple was left as original so that it could be joined by threads to the flange. A photo of the copper heat exchanger connected to the aluminum pipe nipple during assembly is shown in Figure 2-11.

Permatex RTV Sealant was applied to the lip of the aluminum pipe, and the heat exchanger and aluminum pipe were pressed together with a clamp to dry.

Additional sealant was also applied to the outside of the joint for a good seal.

Figure 2-11. Cold heat exchanger connection to aluminum open-ended pipe.

This joint is located on the cooled end and therefore is expected to remain at relatively low temperatures so high temperature sealant was not mandatory. This sealant provided a good watertight seal which was crucial for the cooling method of submersion in an ice/water bath.

When all the pieces were in place, the bolts were tightened carefully while making sure that the device was uniformly straight and that even compression was applied around the circumference of the resonator.

The resonator was checked for leaks by applying Snoop by Swagelok to the seals while pressurizing the inside of the resonator. Snoop is a surfactant formula that is not flammable, has the viscosity of water, and is commonly used to check connections in gas lines for the presence of a leak. To test the resonator for leaks, an air tube fit with a pvc coupling was pressed against the open end of the resonator, with a rubber ring to provide a seal so that air flowed into the resonator to pressurize it. Simultaneously, Snoop was applied to the outside of the seals. Any air leak is made evident by a large amount of extremely tiny bubbles, creating foam around the leak.

This was a helpful test to troubleshoot the device before the operating temperatures were not known. In the unsuccessful tests before the development of the ceramic resonator, it was not known if the device was not producing sound because it was leaking air or if the temperatures were not high enough. This test eliminates the question of air leaks so that the operating temperatures can be tested.

2.1.2. Insulating and cooling

Heat losses to the ambient environment were minimized by insulating the device prior to testing. Kaowool insulation was wrapped around the band heater to deliver most of the heat from the heater into the hot heat exchanger. On the cold end, insulation was also wrapped around the ice as well as possible to minimize melting of the ice or heating of the cooling water from the ambient environment.

A cooling method was used which contained the cold heat exchanger in an ice/water bath. This was done by cutting a 25.4 mm diameter circle in the bottom of a Styrofoam cup and trimming the cup height to be about 25 mm so that it fit within the clearance of the compression rods. The cup was fit around the cold heat exchanger snugly and sealed with Permatex RTV Sealant. A 6.35 mm water tube, 150 mm long, was sealed into a hole in the upper side of the cup for water drainage to an outside cup as shown in Figure 2-12.

Figure 2-12. Cooling method for cold heat exchanger.

Before and during each test, small ice cubes and chunks of ice were place into the cup along with some water to ensure good thermal contact with the copper. As the ice melted during testing, additional ice was placed continuously into the cup as excess water was drained through this tube to prevent overflow. The ice/water mixture was mixed at intervals during the test to keep the cold heat exchanger submerged in contact with a cold environment.

This attachment was done prior to assembly of the resonator, after the cold heat exchanger was sealed to the aluminum pipe nipple.

2.2. Test Procedures

The device was tested under different heating conditions corresponding to full power and reduced power from the band heater to determine the necessary temperature difference, mean operating temperature and power input required for both the onset of sound and the sustainment of sound.

Before each test, the cooling cup was filled with ice and water to submerge the outside of the cold heat exchanger in an ice/water bath. Kaowool insulation was wrapped around the band heater and stack holder to minimize heat losses. Insulation was also wrapped around the cooling portion to minimize the ice melting from the ambient environment.

Two thermocouples were used to measure temperatures at the hot and cold portions of the device. Thermocouple #1 was placed on the outside surface of the copper ring on the hot heat exchanger. It was positioned so that the thermocouple bead was touching the copper underneath the edge of the band heater. Thermocouple #2 was pushed from the open end of the resonator into the copper foam of the cold heat exchanger. This thermocouple was a type-K thin wire thermocouple 305 mm in length and with a diameter of 0.254 mm. The temperatures were recorded at intervals of 10 seconds during heatup, and the temperatures and times of sound onset were also recorded.

To measure the temperatures inside the device, a thermocouple with a diameter of 0.254 mm was threaded through the inside centerline of the resonator.

Markings along the thermocouple had been made to denote each location upon the withdrawing of the thermocouple. After steady-state, the thermocouple was pulled out slowly to record temperatures at each component within the device. Unfortunately, the thermocouple could not be threaded through the two heat exchangers and stack from the open end of the resonator, so the resonator was taken apart and the thermocouple was threaded through each component one by one. The thermocouple tip was inside the closed end of the resonator, at x=0.

Sound measurements were taken using a sound level meter (Model SL-4001 by Lutron) shown in Figure 2-13. The microphone was positioned 38 mm from the open end of the resonator on the centerline of the x-axis.

To determine the minimum temperatures at sound onset, Design #1 was tested at a power input of 62 W, corresponding to full heater power. The band heater was turned on and the temperatures up to onset and at sound onset were recorded. In each of these tests after the first onset of

Figure 2-13. Sound level meter used to measure decibel level.

sound, the power was shut off and the tone was allowed to cease. At this point, the heater was plugged back in at full power and the sound resumed after about 30 seconds of reheating. This cycle was repeated a few times during each test to establish a range of temperatures at onset as well as hot heat exchanger heatup rates prior to sound onset.

Tests were done with Design #1 to determine the critical power level for sound onset using a variable transformer to reduce heater power. These tests

began with a low power input of 24 W, corresponding to a heater power level of 40%. When the hot end temperature was steady with no sound occurring for 2 minutes, the power input was increased in 10% increments until the onset of sound occurred. Then an additional the test was done in which the device was heated at this critical power level until sound onset.

Tests were also done with Design #1 to determine the critical power level for sound continuation post-onset. First, the heater was turned on at full power, corresponding to 62 W. After the onset of sound, the power was reduced to 19 After the sound stopped, the power was slowly increased to 31 W, then after 2 minutes of no sound, was increased to 62 W, resulting in a second onset of sound. Within 5 seconds, the power was again reduced to 31 W and the tone continued at a steady-state hot-end temperature for 4 minutes, indicating the critical level for steady-state sound continuation.

For comparison, two tests were done at full heater power to sound onset for Design #2. The power input corresponded to 47 W because of the reduced outer surface area of the smaller heat exchanger in contact with the band heater. The heatup rates of the hot heat exchanger were also recorded for comparison and were identical to those in tests with Design #1. These tests also recorded the total time of the tone from onset to cessation when the power is left on for 15 seconds post-onset and when it is shut off immediately upon sound onset.

3. Results and Analysis

The power input to the hot heat exchanger was estimated based on the surface area of the band heater in contact with the outside copper surface of the hot heat exchanger, which was $1267\ mm^2$ for Design #1 and $950\ mm^2$ for Design #2. The heater wrapped around the circumference with the exception of a 5 mm gap where the wiring was located. The length was in contact with the heat exchanger for a length of 17 mm in Design #1, and 12 mm in Design #2. The heater power density at full power was $0.0496\ W/mm^2$. This corresponded to a maximum power input of 62 W for Design #1 and 47 W for Design #2.

Kaowool insulation was wrapped around the band heater and hot heat exchanger to minimize losses to the ambient. This insulation layer was about 20 mm thick and became slightly warm from the heating during the tests, but not hot. For estimation of the power input from the heater into the device, heat losses were neglected. However, heat losses may have slightly lowered the actual power input by about 5 W.

The measurements for T_{hot} and T_{cold} correspond to the temperatures of the heat exchangers on either side of the stack. T_{hot} was measured with thermocouple
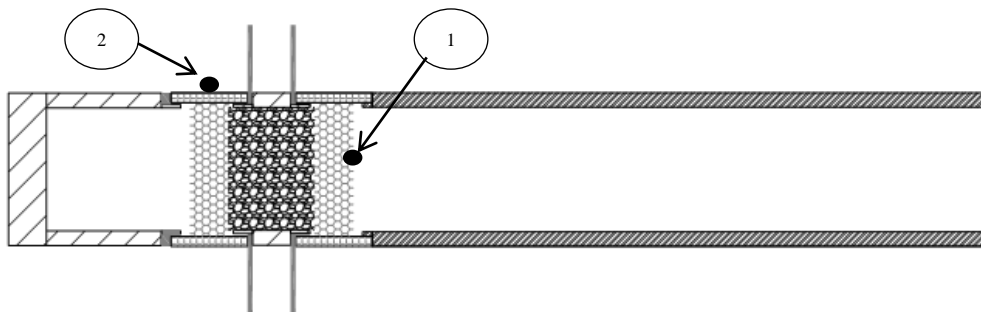

Figure 3-1. Locations of thermocouple measurements.

#2 as shown in Figure 3-1. This thermocouple was touching the outside copper ring surface of the hot heat exchanger under the band heater. The inside copper foam heat exchanger temperature was assumed to be within $5-10\,°C$ of this surface based on the heatup evaluation of the heat exchanger prior to the device assembly. T_{cold} was measured with thermocouple #1 as shown in in Figure 3-1. This thermocouple was touching the copper foam surface in the cold heat exchanger. These locations were chosen to evaluate the temperature difference across the stack and were the simplest locations for the thermocouples after device assembly.

The estimated error for the temperature measurements is $10\,°C$. This is based on evaluating the contact of the thermocouples with the copper as well as the response time. The thermocouple bead might not have always been in good contact with the copper, and at points may have been reading the gas temperatures instead. A better way to ensure contact would have been to solder the thermocouples to the copper surfaces. Also, the thermocouple response time could have been improved by using thinner thermocouples with smaller beads.

At the full power setting, the outside surface of the hot heat exchanger experienced a heatup rate of $\sim 1.9\,°C/s$, which was calculated as the slope of the hot-end temperature from $t = 50\ to\ t_{onset}$ because this was the most linear region of the temperature increase as a function of time. Likewise, the heatup rate of the cold heat exchanger was also calculated in this way and varied based on the level of cooling.

With an input power of 62 W to Design #1, the sound occurred on average with a cold end temperature of $T_{cold} = 129\,°C$ and hot end temperature of $T_{hot} 299\,°C$. This corresponds to a temperature difference of $\Delta T = 170\,°C$ across the stack, a critical temperature gradient of $\nabla T = 85\,°C/cm$, and mean operating temperature of $T_m = 214\,°C$.

By varying the power input to the hot heat exchanger it was found that there is a critical power level below which the sound onset will not occur. Also, after sound onset, there is a critical power level necessary to sustain the sound. These two power levels were found to be different. The critical power level for steady-state operation was 31 W, and for sound onset was 44 W. Steady-state was maintained with $T_{hot} \approx 310\,°C$ and $T_{cold} \approx 155\,°C$, corresponding to $\Delta T_{ss} \approx 155°C$, $\nabla T_{ss} \approx 78\,°C/cm$ and $T_{m,ss} \approx 217\,°C$.

For comparison of temperatures at sound onset, Design #2 was tested at full heater power, corresponding to 47 W. This design showed an improvement, producing sound at lower hot heat exchanger temperatures than Design #1. The average temperatures at the onset of sound for the hot heat exchanger was $T_{hot} = 267\,°C$ and the cold heat exchanger was at $T_{cold} = 162°C$. This corresponds with a critical temperature difference of $\Delta T = 169\,°C$, a critical temperature gradient of $\nabla T = 70\,°C/cm$ and a mean temperature of $T_m = 213\,°C$.

3.1. Onset of Sound

Tests were done to establish the temperature at which the onset of sound occurs using the full heater power, which corresponds to 62 W into the copper of the hot heat exchanger.

The band heater was turned on at this power until the sound began. During the first test, the sound occurred when the hot heat exchanger temperature reached 308 ℃, (cold heat exchanger at 117 ℃). Within 5 seconds, the heater was unplugged and the tone continued for about two minutes. It stopped when the hot end temperature decreased to 292 ℃ (cold heat exchanger at 110 ℃). The heater was plugged back in, and upon reaching 298 ℃ (cold heat exchanger at 113 ℃), the sound resumed. This cycle of heating was repeated 5 times to establish what the minimum temperatures needed to be for the tone to be produced at this power input. Five tests were run to establish criteria at the first onset of sound, and the first three tests included this reheating cycle.

The cold end was cooled using ice-water as described previously, but the cold end temperatures still increased at an average of $0.5\ ℃/s$. The temperatures at the first onset of sound on average when the hot heat exchanger reached
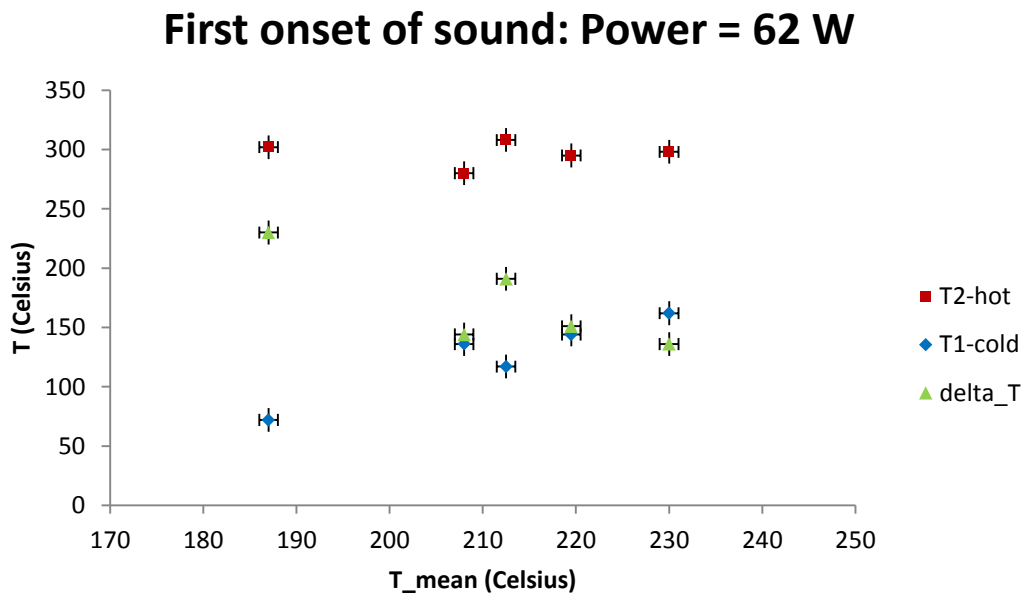

Figure 3-2. Temperatures at first onset of sound, P = 62 W.

$T_{hot} = 297\,°\text{C}$ and the cold heat exchanger was at $T_{cold} = 126\,°\text{C}$. This corresponds with a critical temperature difference of $\Delta T = 170\,°\text{C}$, a critical temperature gradient of $\nabla T = 85\,°\text{C}/cm$ and a mean temperature of $T_m = 211°\text{C}$. The results for each test at the first onset of sound are plotted in Figure 3-2.

In each of these tests after the first onset of sound, the power was shut off and the tone was allowed to cease. It was noted that the tone did not immediately cease upon power shutoff, and continued for up to 2 minutes before dying out. At this point, the heater was plugged back in at full power and the sound resumed after about 30 seconds of reheating.

This cycle was repeated a 3-5 times during each test. A comparison of the average temperatures at the first sound onset and at the subsequent sound onsets during the reheating cycle are tabulated in Table 3-1. These do not show a significant difference in sound onset temperatures when heating from rest versus reheating at a constant power level, indicating that these are the required temperatures for the onset of sound for the device configuration at this power input level.

	T_{cold} (°C)	T_{hot} (°C)	ΔT (°C)	∇T_{crit} (°C/cm)	T_{mean} (°C)
First onset	126.2	296.6	170.4	85.2	211.4
Reheating	131.9	301.3	169.4	84.7	216.6

Table 3-1. Comparison of average values during reheating cycle at P=62 W.

This gives the critical temperature gradient as $\nabla T = 85\,°\text{C}/cm$, and mean operating temperature of $T_m = 214\,°\text{C}$ for the onset of sound. This corresponds to a temperature difference of $\Delta T = 170\,°\text{C}$ across the stack, with a cold end temperature of $T_{cold} = 129\,°\text{C}$ and hot end temperature of $T_{hot} = 299\,°\text{C}$.

3.2. Steady-State

A test was done to establish the steady-state operating temperatures and power input by varying the power to the heater. The temperatures are shown at each time in Figure 3-3 indicating in order when the power was increased or decreased. The points at which the sound began and stopped are marked with double lines and

Establishment of steady-state

Figure 3-3. Establishment of steady-state temperatures.
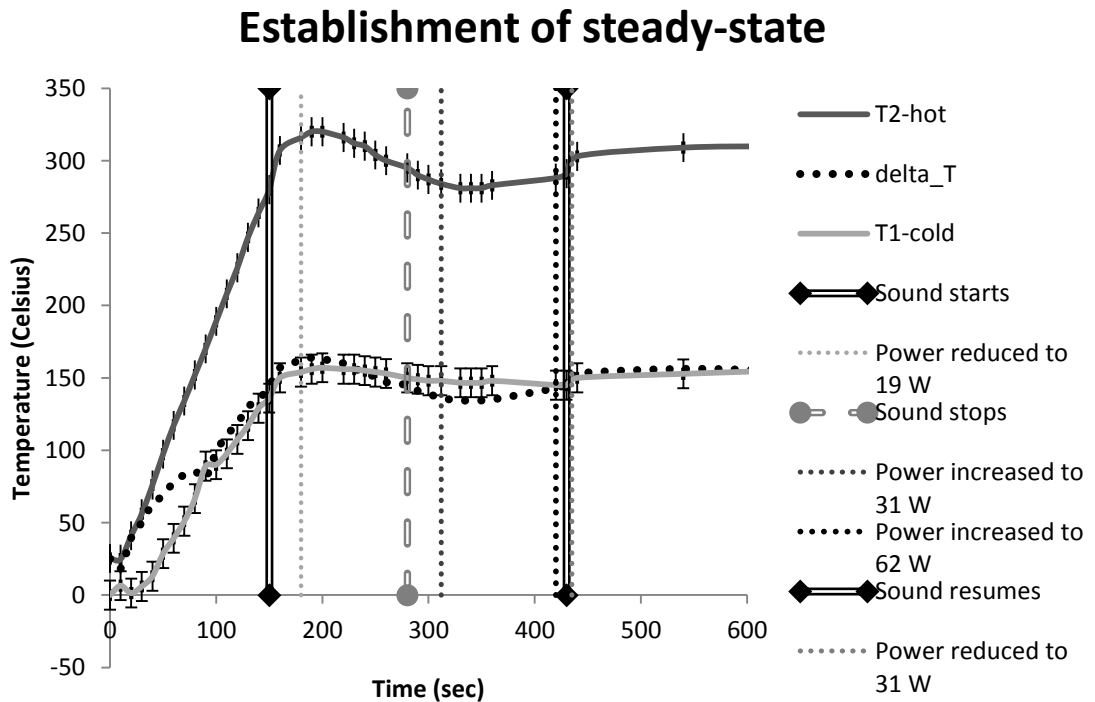
dashed lines, respectively.

First, the heater was turned on at full power, corresponding to 62 W. The sound began at 150 seconds with a hot end temperature of $T_{hot} = 280\ ^\circ\text{C}$ and a temperature difference of $\Delta T = 144\ ^\circ\text{C}$. The power was then reduced to 19 W at 180 seconds. Then 100 seconds after the power was reduced, the sound ceased at

280 seconds. At the point of sound cessation, the hot end temperature was $T_{hot} = 295\,°C$ and the temperature difference was $\Delta T = 145\,°C$.

Thirty seconds after sound cessation, the power was increased to 31 W. During this heating period, the temperatures leveled out, with the hot end temperature at $T_{hot} = 288\,°C$ and a temperature difference of $\Delta T = 143\,°C$. Sound was still not being produced. The temperature was increased to 62 W at 420 seconds, and within 10 seconds of the increase in power, the sound resumed, indicated by the second double line in Figure 3-3. This occurred at 430 seconds, with a hot end temperature of $T_{hot} = 291\,°C$ and a temperature difference of $\Delta T = 146\,°C$. Within 5 seconds of this sound onset, the power level was reduced to 31 W and remained there for 4 minutes with the tone continuing.

It was observed that in previous tests when the power was shut off, the sound continued for up to 2 minutes, depending on the power level and amount of time that the power was kept on after the sound began. In this case with the steady-state sound oscillation sustained with a power level at 31 W, the sound continued indefinitely, indicating that the external power was driving the sound and not the residual heat stored in the copper foam of the hot heat exchanger.

At this power input, the temperatures were held constant at $T_{hot} \approx 310\,°C$ and $T_{cold} \approx 155\,°C$. The sound was sustained at a level of ~108 dB. The critical temperature difference for sustainment was $\Delta T \approx 155\,°C$, corresponding to a critical temperature gradient of $\nabla T \approx 78\,°C/cm$ at a mean operating temperature of $T_m \approx 230\,°C$. A summary of the criteria for steady-state operation is provided in Table 3-2.

Power (W)	T_{cold} (°C)	T_{hot} (°C)	ΔT (°C)	∇T_{crit} (°C/cm)	T_{mean} (°C)	Sound (dB)
31	150	310	155	78	230	108

Table 3-2. Steady-state operation criteria for continuation of sound.

The centerline temperatures within the resonator were measured at steady state using a long thermocouple with a diameter of 0.254 mm. The device was heated full power and upon sound onset was reduced to 31 W in an attempt to attain steady-state temperatures.

However, during withdrawing of the thin thermocouple, the outside hot temperature reached $T_{hot} = 406$ °C so this was recorded as the upper bound. This test was repeated and the average of the recorded temperatures are plotted as a function of x in Figure 3-4. The solid horizontal lines denote the temperatures at the outer surfaces of the hot heat exchanger and copper foam of the cold copper heat exchanger.
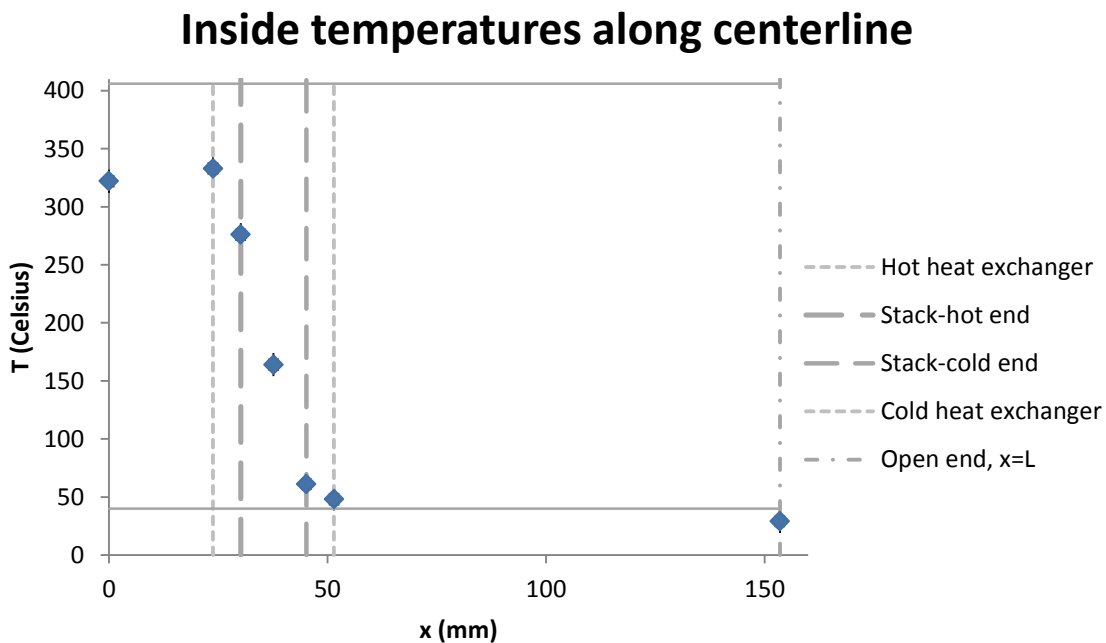

Figure 3-4. Temperatures along centerline of resonator.

Although the outside temperatures are higher than in the previous tests, this gives an example of the temperature profile within the device along the centerline.

In a thermoacoustic device, the gas parcel temperature does not exactly match the solid surface temperature. This allows for oscillating heat transfer to occur between the solid and the gas, such that in the hot region, the solid is hotter than the gas and therefore transferring heat to the gas. In the cooler region, the gas is warmer than the solid and transfers heat to the solid [11]. In this case, it makes sense that the hot heat exchanger is at $T_{hx,hot} \approx 400\ ℃\ to\ 333\ ℃$, based upon the measurements from the outside copper surface and inside gas or foam surface within the hot heat exchanger. The corresponding gas temperature in the hot region of the stack is slightly cooler, at $T_{stack,hot} \approx 276℃$ as heat is being transferred from the hot heat exchanger and hot end of stack into the gas. Within the center of the stack, $T_{x_{stack}} \approx 164℃$ and at the cold end $T_{stack,cold} \approx 61℃$, as the air is transferring heat to the cooler portion of the stack and adjacent cold heat exchanger. At the open end of the tube, not much heat is being transferred here and the temperature is about ambient at $T_{x=L} \approx 29℃$.

At the closed end, $T_{x=0} \approx 322\ ℃$. This is slightly lower than the temperature recorded in the region of the copper foam of the hot heat exchanger, which was $T_{hx,hot} \approx 333\ ℃$. The temperature at the closed end would depend on how long the device had been heating. In this case, it was at steady-state and $T_{x=0} \approx 322\ ℃$ due to the heat transfer convecting from the hot heat exchanger.

But this would be expected to be lower at the point of sound onset, as the heat would not have had as much time to collect in this region yet.

The temperatures along the centerline inside the device were obtained at steady-state. Although the temperature of the outer surface of the hot heat exchanger had increased to 405 °C in this test and only needed to be ~300 °C for the onset of sound and 310 °C if the power is able to be accurately controlled, this would give a better profile of the air temperatures at steady-state within the device.

3.3. Critical Power for Onset of Sound

The critical temperatures and power input for the onset of sound were determined by initially heating the device at a low power level. If the temperature reached a steady value without an onset of sound, the power level was increased slightly.

First the heater was turned on 40%, corresponding to a power input of at 25 W. After 285 seconds, the hot end temperature was steady at $T_{hot} = 299$ °C and no sound was occurring. Therefore the power input was increased to 38 W. After a total time of 505 seconds, the hot end temperature was steady at $T_{hot} = 326$ °C and still no sound was produced. The power was increased to 44 W, and within 10 seconds the sound occurred at a hot end temperature of $T_{hot} = 326$ °C.

The test was repeated at a constant power input of 44 W. The onset of sound occurred at $T_{hot} = 305$ °C, $T_{cold} = 150$ °C and $\Delta T = 150$ °C at a time of 340 seconds.

Comparison of power inputs
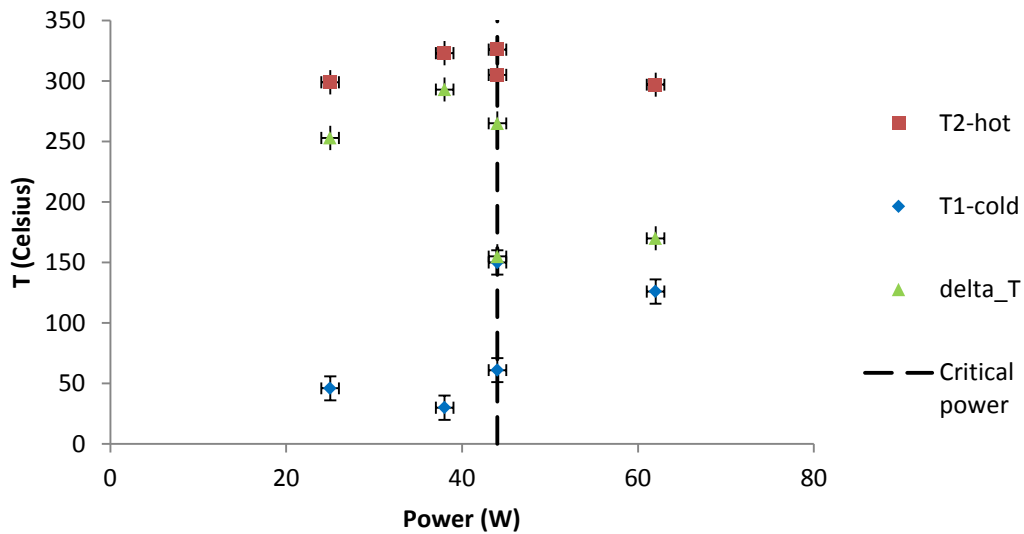
Figure 3-5. Critical power input for onset of sound.

The results are plotted in Figure 3-5, indicating temperatures at the onset of sound and the critical power level for onset. Below the critical power level of 44 W, sound did not occur even though the temperature difference was above that for sound onset.

This implies that in addition to the temperature gradient across the stack, a minimum power input is needed to cause the onset of sound. Tests were conducted using the Pyrex tube resonator at varying power levels while measuring the temperature gradient across the stack with $\Delta x_{stack} = 25.4$ mm. The temperature gradient across the stack is plotted for each power level in Figure 3-6.

In the Pyrex tube resonator, 28 W was the critical power level below which sound onset would not occur. Between the power levels from 28 W to 33.3 W, the sound onset occurs but was not sustainable as it died out

within 2 minutes of onset. Here, the temperature gradient at sound cessation was much higher than that at sound onset, and was slightly below the steady-state value. Above 33.3 W, the sound was sustained.

From the values above corresponding to the Pyrex tube resonator, it can be seen that with lower power inputs, a higher gradient is required at sound onset. These lower power inputs also produce lower steady-state gradients, due to the lower temperature of the resistance wire. For the critical power level of 33.3 W, the gradient at sound onset was 18 ℃/cm and the gradient at steady-state operation was 135 ℃/cm. Comparatively, at the higher power of 41.5 W, the gradient at sound onset was 20 ℃/cm, while at the lower powers, the gradient at
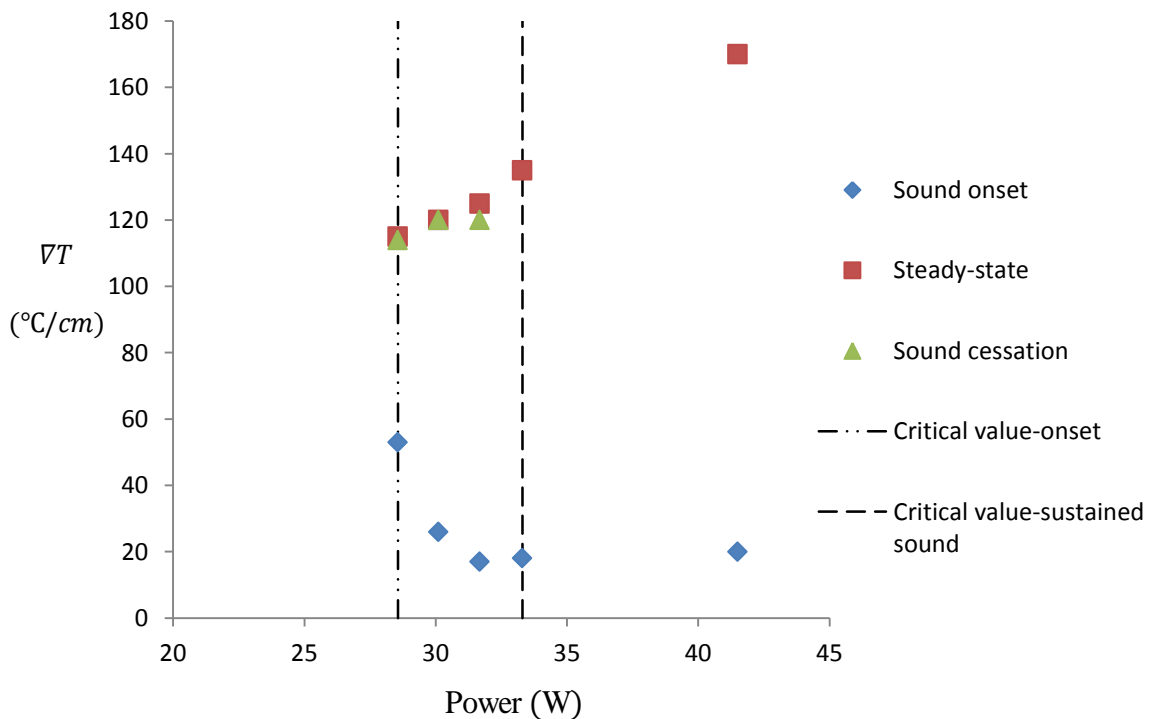

Figure 3-6. Temperature gradient across stack vs. power input, Pyrex tube resonator.

sound onset ranged from $26 - 53\,°C/cm$. From this assessment of the Pyrex tube resonator, the critical temperature gradient at sound onset for the configuration was $17\,°C/cm$, and at steady-state was $135\,°C/cm$.

The resistance wire in the Pyrex tube resonator immediately heats up to provide heat input directly to the hot end of the stack. In the design of the prototype flashover detector, the external surface of the hot heat exchanger is heated, producing a much slower heatup rate to the hot end of the stack. The onset of sound occurred within 5 seconds for the Pyrex tube resonator, and at 150 seconds on average for the prototype flashover detector. To compare minimum power inputs of the two devices, the steady-state temperatures from the Pyrex tube tests will be compared with the onset temperature from the prototype flashover detector.

The minimum power input for sound onset in Design #1 is compared to those for the Pyrex test tube resonator in Figure 3-7. The critical power level for Design #1 with $\Delta x_{stack} = 20\,mm$ was 47 W, compared to 33 W for the Pyrex tube resonator was $\Delta x_{stack} = 25.4\,mm$. This could have been due to heat losses from the outside of the hot heat exchanger to the inside surface in contact with the stack in the prototype design resonator. Also, there may have been an increase in viscous losses at the junctions of the components of prototype design resonator, compared with the one-piece design of the Pyrex tube resonator. However, the temperature gradients were very similar, with $\nabla T = 135\,°C/cm$ for the Pyrex tube resonator and $\nabla T = 133\,°C/cm$ for Design #1.

Temperature gradient vs. Critical power level for sound onset
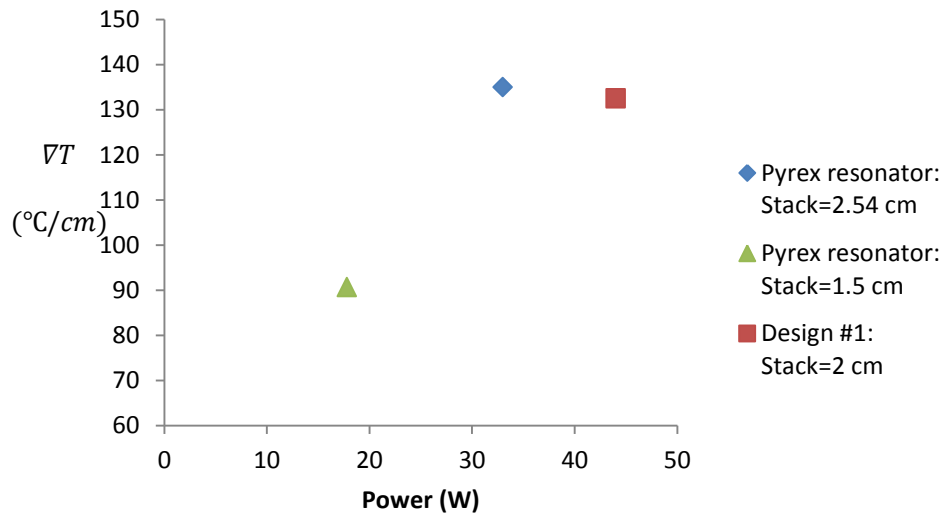
Figure 3-7. Comparison of critical power levels for sound onset with Pyrex tube resonator.

It was observed in the Pyrex tube resonator that by reducing the stack length from $\Delta x_{stack} = 25.4\ mm$ to $\Delta x_{stack} = 15\ mm$, the critical power level for sound onset was reduced from 33.3 W to 17.8 W. This indicates that a shortening the stack can produce sound at lower power levels and follows the trend by which Symko and McLaughlin were able to produce sound at power levels of 2 W in a much smaller resonator with a total length of 2 cm [22].

3.4. Cooling of Cold Heat Exchanger

While the Pyrex tube resonator successfully operates without a cold heat exchanger, the rapid heat input from the resistance wire to the stack makes the sound possible by producing a temperature gradient across the stack. In the prototype flashover detector, the heatup rate is much slower due to heat transfer from the external surface of the hot heat exchanger to the inside surface of the

copper foam. For comparison, the heatup rate of the hot end of the stack is estimated as ~21 ℃/s from the resistance wire at 33 W in the Pyrex tube setup, increasing to 65℃ in 3 seconds at sound onset. In the prototype flashover detector, the heatup rate of the hot heat exchanger is ~1.9 ℃/s at 44 W from the band heater, corresponding to an even slower heatup rate of the hot end of the stack, which was not measured.

A fixed-temperature cool heat exchanger would keep the cold end of the stack at a constant temperature, allowing only for heatup of the hot end from the radiant heat from the fire. This would make the onset of sound for the device more quantifiable so that it would be an accurate warning system for firefighters at the onset of flashover.

In the tests, the cold heat exchanger was submerged in an ice/water bath. If the ice was allowed to melt during a test, the water temperature could rise up to 99℃. If additional ice was continually added, the water temperature remained around 10℃. The corresponding outer surface of the cold copper heat exchanger was hotter than the water temperature. The inner surface of the copper foam of this heat exchanger was hotter than the outside copper temperature due to the heat transfer within the resonator.

The average temperatures of the water and copper foam heat exchanger are plotted in Figure 3-8 for the start and end of each test. In the plot, x=0 corresponds with the center of the copper foam within the cold heat exchanger. The measurement goes outward radially, such that x=12.7 corresponds with the outer surface of the copper, beyond which is the ice/water mixture which was

Increase in cold heat exchanger temperature
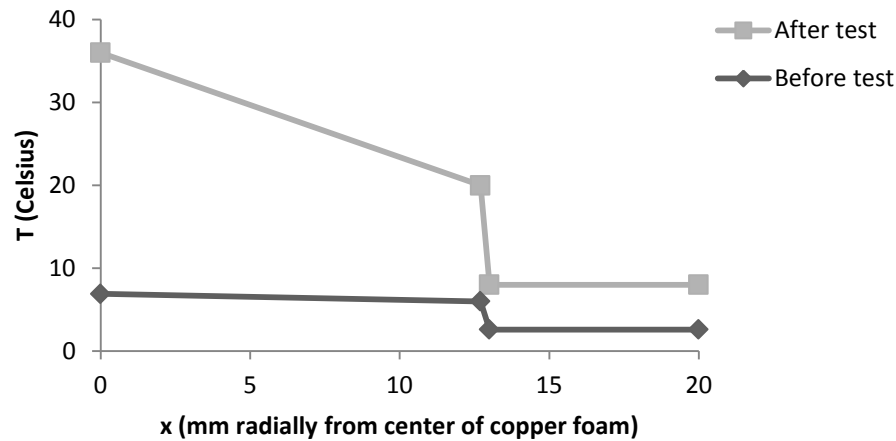
Figure 3-8. Cold heat exchanger temperatures at beginning and end of test with ice.

assumed to be at a relatively constant temperature. At the beginning of the test, the water temperature was $2.6\,℃$, which rose to $8\,℃$ at the end of the test. Meanwhile, the inside surface of the copper foam rose from $7\,℃$ to $36\,℃$ during the test.

If the ice was allowed to melt during the test and was not replaced with more ice, the water temperature rose to $\sim 50\,℃$. The corresponding inside cold heat exchanger temperature was typically in the range of $117 - 155\,℃$ while the device was producing sound and the hot end temperature was kept between $295 - 308℃$.

Tests were done using Design #1 with the power at 62 W and at 44 W under different cooling conditions to assess whether the onset of sound could occur at lower hot-end temperatures, given the temperature difference of $\Delta T \approx 160\,℃$.

These different cooling setups included ice/water which was allowed to melt during heatup, a mixture of dry ice and water, and a mixture of ice and water in which ice was continuously added during heatup to keep cold end temperatures low.

It was found that with cooling to keep the cold-end temperature below ~60 °C, the hot-end temperature at the point of sound onset was not lower than the tests without this level of cooling. The temperatures are plotted as a function of temperature difference at onset in Figure 3-9 for tests at power inputs of 44 W and 62 W for Design #1. This trend was consistent for both power levels and shows a higher temperature difference needed with the lower cold-end temperatures.
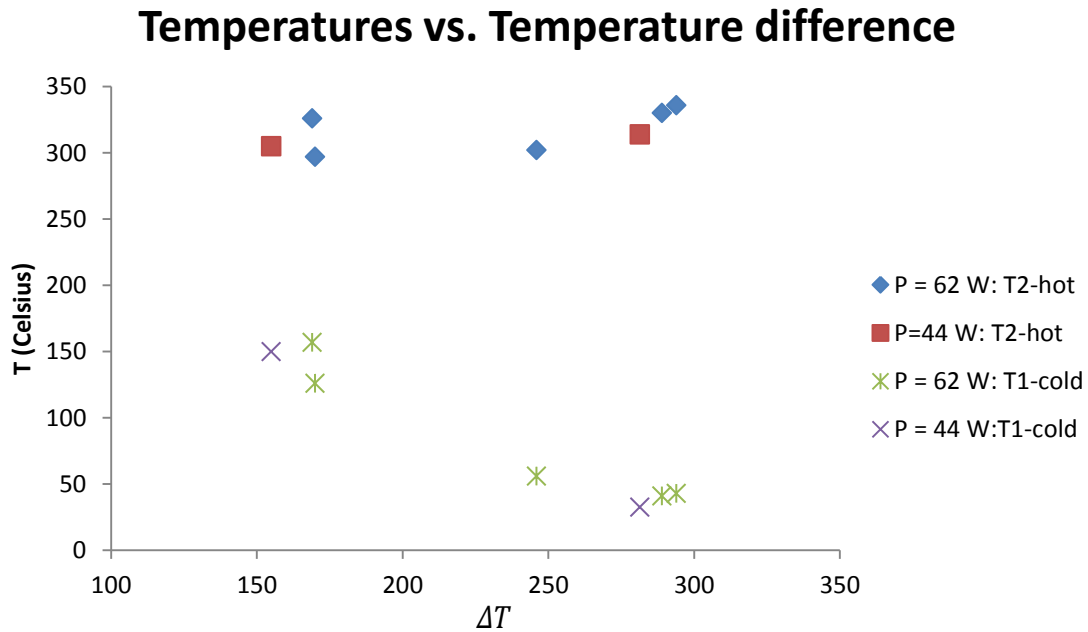
Figure 3-9. Temperatures vs. temperature difference at onset of sound at power levels.

3.4.1. Mean Operating Temperature

In addition to the temperature gradient across the stack, the mean temperature across the stack appears to play a role in the onset of sound. In the tests where the cold heat exchanger was kept cooler by continuing to replace ice as it melted, the onset of sound did not occur at lower hot-end temperatures; it actually occurred at slightly higher hot-end temperatures. The hot and cold temperatures at the onset of sound are plotted along with the mean temperature in Figure 3-10. This data was from Design #1 with a power input of 62 W, corresponding to a hot end heatup rate of $\sim$1.8 $°C/s$.

The trend in Figure 3-10 shows that the temperature difference alone is not indicative of the sound. A temperature difference of $\Delta T = 170\,°C$ between $T_{hot} = 297\,°C$ and $T_{cold} = 126\,°C$ produced sound, but lowering the cold

Figure 3-10. Temperature at sound onset vs. mean temperature, P = 62 W.

temperature to $T_{cold} = 56\,°C$ did not correspond to sound occurring at $T_{hot} =$ 226 °C. With this lower cold end temperature, the sound did not onset until $T_{hot} = 302\,°C$. Likewise, for $T_{cold} = 41\,°C$ and $T_{cold} = 43\,°C$, the hot temperatures at sound onset were $T_{hot} = 330\,°C$ and $T_{hot} = 336\,°C$ respectively.
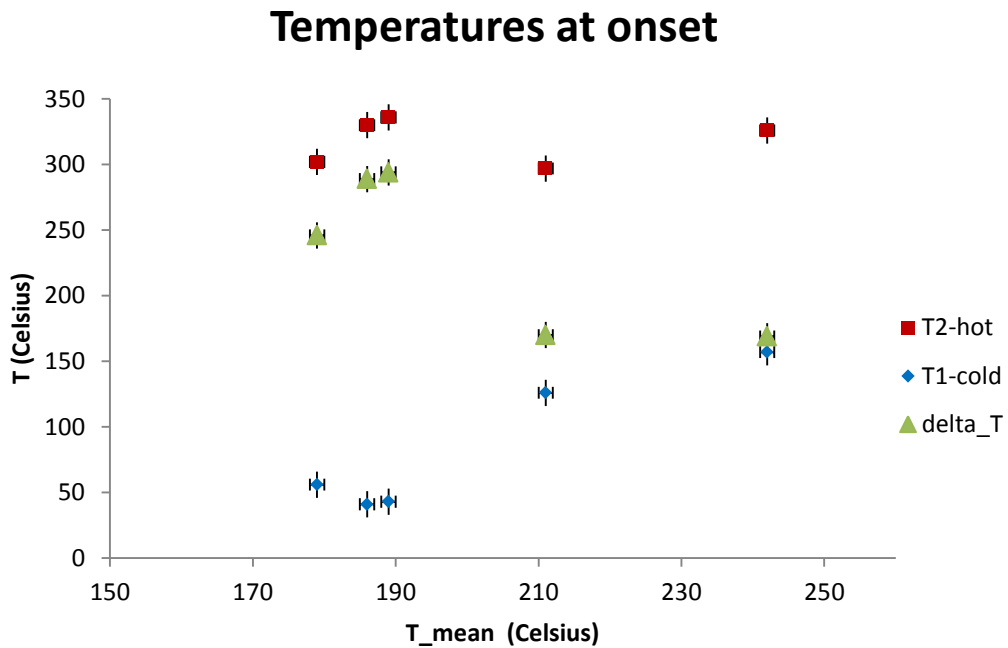
The hot heat exchanger temperature at onset in these tests ranged from $296 - 336\,°C$, while the mean temperature ranged from $173 - 227\,°C$. It would be expected that a lower mean temperature would correspond with a lower hot-end temperature, but this does not appear to be the case. Lower mean operating temperatures appear to correspond with higher temperature differences for the onset of sound to occur. This suggests a dependence on a critical value for the mean operating temperature or hot end temperature. If the onset of sound is dependent on the mean operating temperature, it appears that the critical value is around $T_m = 173\,°C$. If it is dependent on the hot end temperature, the critical value would appear to be about $T_{hot} \approx 300\,°C$.

It is interesting to evaluate the thermal boundary layer depth at these mean temperatures. Evaluating equation 1-11 at increasing temperatures shows that the thermal boundary layer slightly increases from $\delta_K \approx 0.17\,mm$ at 173 °C to $\delta_K \approx 0.19\,mm$ at 227°C. Thus it is likely that at higher mean operating temperatures, the fibers of the stack with the current spacing and density are better able to heat the air to produce the necessary gas oscillations.

If the stack is modeled as parallel plates, the distance between the plates should be on the order of $2\delta_K$ [9]. This introduces the possibility of altering the spacing between the stack plates or fibers such that it is closer to the

corresponding values of $2\delta_K$ at $T = 173\ °C$ or lower. Although the stack utilized in the design is a random cylinder of steel wool, it is possible that with a more densely packed stack, different fiber thickness, or alternate stack material corresponding to a prescribed spacing distance, the mean operating temperature could be reduced.

3.5. Comparison of Designs #1 and #2

Swift indicated that the temperatures for operation are a function of the geometry and materials of the device [9]. As the operation parameters for the device are dependent heavily on the materials and geometry, the temperatures may be able to be reduced with a smaller, optimized design with optimal stack positioning.

Design #2 was built and tested at full heater power to compare the temperature at which the onset of sound occurs for these dimensions. The power input corresponded to 47 W due to the reduced outer surface area of the hot heat exchanger in contact with the band heater. But the average heatup rate of the outside of the hot heat exchanger was $\sim 1.9\ °C/s$, identical to that of the tests at full heater power in Design #1. For the cold-end with water/ice cooling, the average heatup rate was $0.75\ °C/s$.

The average temperatures at the onset of sound for the hot heat exchanger was $T_{hot} = 267\ °C$ and the cold heat exchanger was at $T_{cold} = 162\ °C$. This corresponds with a critical temperature difference of $\Delta T = 169\ °C$, a critical temperature gradient of $\nabla T = 70\ °C/cm$ and a mean temperature of $T_m = 213\ °C$.

A summary of the average temperatures of the outside copper of the hot heat exchanger and inside copper foam of the cold heat exchanger at the onset of sound for Designs #1 and #2 is provided in Table 3-3.

	T_{hot} (°C)	T_{cold} (°C)	ΔT (°C)	∇T (°C/cm)	T_m (°C)
Design #1: P = 62 W (sound onset)	301	132	169	84.5	214
Design #2: P = 47 W (sound onset)	267	162	105	70	215

Table 3-3. Comparison of Designs #1 and #2.

The temperature of the hot heat exchanger at the onset of sound was 34 °C lower in Design #2 than in Design #1 with the same stack density and hot heat exchanger heatup rate. This is a significant difference, which could be due to a combination of factors. The shorter stack could have decreased the amount of time needed to reach the mean temperature of 215 °C by heating the cold heat exchanger to a higher temperature. However, in a test with only water cooling in Design #1, the cold heat exchanger was allowed to reach $T_{cold} = 156$ °C but the onset of sound did not occur until $\Delta T = 170$ °C with $T_{hot} = 326$ °C at $T_m = 241$ °C. A more likely possibility is that the geometry of the device is better in Design #2.

The position of the stack within the resonator may have an effect on the temperatures and powers needed for sound onset. Jung and Matveev experimented with different stack positions by varying the overall resonator length, resulting in different values of $\frac{x_{stack}}{L}$ as well as different critical temperatures at onset. The lowest temperature difference required for sound onset

occurred when $\frac{x_{stack}}{L} = 0.18$ [13]. In this project, Design #1 had $\frac{x_{stack}}{L} = 0.34$

and Design #2 had $\frac{x_{stack}}{L} = 0.22$.

Although the design tested by Jung and Matveev is smaller than the

designs tested in this project, the ratios of resonator length to inner diameter ($\frac{L}{ID}$),

stack center position from closed end ($\frac{x_{stack}}{L}$), and overall stack length with

respect to resonator length ($\frac{\Delta x_{stack}}{L}$) are comparable.

In Jung and Matveev's experiments, the lowest critical temperature

difference occurred with $\frac{x_{stack}}{L} = 0.18$. Similarly, in the experiments described in

this thesis, the lowest critical temperature difference occurred with $\frac{x_{stack}}{L} = 0.22$

in Design #2. This suggests an ideal stack center position of $\frac{x_{stack}}{L} \approx 0.20$. This is

in agreement with the stack location being positioned at $\frac{\lambda}{20}$ in a quarter-length

resonator [8].

A plot comparing stack location with respect to resonator length and the

temperature difference at onset is shown in Figure 3-11. This includes data from

the experiments in this thesis, as well as data from Jung and Matveev's

experiments [13].

Shorter stack lengths also correspond to lower power levels and critical

temperature gradients. There is also likely an ideal stack length for a given set of

resonator dimensions and stack placement. In the test with the lowest critical

temperature in Jung and Matveev's experiments, $\frac{\Delta x_{stack}}{L} = 0.07$. In the

experiments done in this project, the lowest critical temperature occurred with
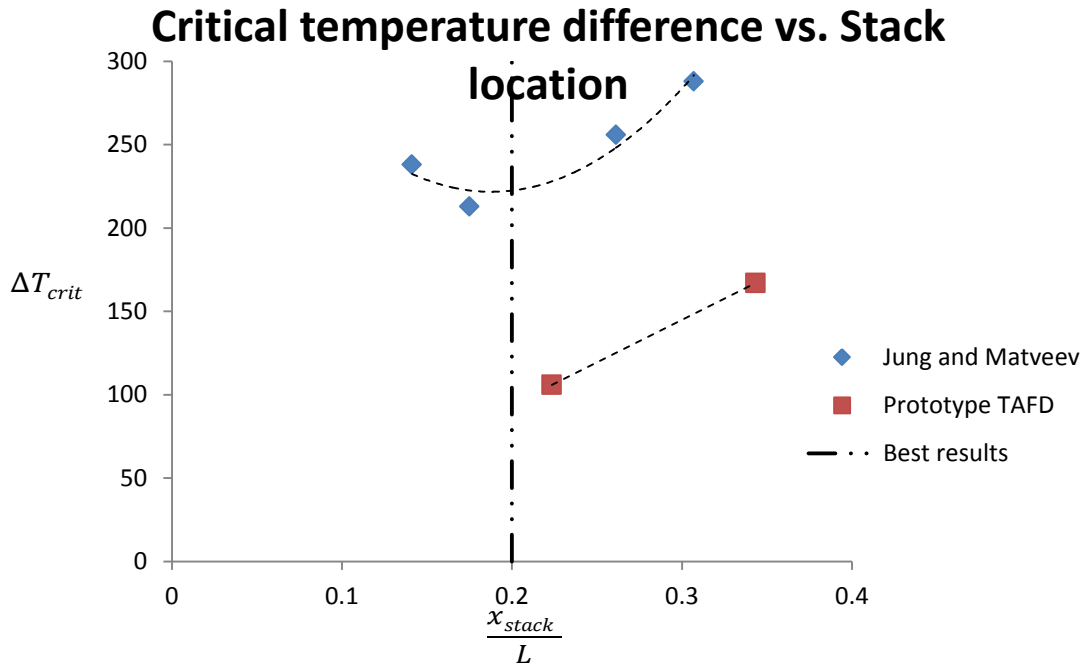
Figure 3-11. Comparison of temperature difference at onset vs. stack center location [13].

$\frac{\Delta x_{stack}}{L} = 0.09$ in Design #2, but there was not much variation in overall stack length with respect to resonator length for Design #1 and Design #2, as Design #1 had $\frac{\Delta x_{stack}}{L} = 0.10$.

Furthermore, utilizing a shorter stack will most likely require lower power inputs as confirmed in testing with the Pyrex resonator tests. By reducing the size of the stack from $\Delta x_{stack} = 25.4\ mm$ to $\Delta x_{stack} = 15\ mm$, the required power input for sound was reduced from 33.3 W to 17.8 W. The corresponding decrease in $\frac{\Delta x_{stack}}{L}$ was from $\frac{\Delta x_{stack}}{L} = 0.15$ to 0.07.

Also in shortening the stack, the temperature gradient at sound onset does not appear to change significantly. From Design #1 to Design #2, the temperature difference was reduced from $\Delta T_{crit} = 167\ °C$ to $\Delta T_{crit} = 106\ °C$. Meanwhile, the

temperature gradient across the stack was only slightly reduced from $\nabla T_{crit} = 85\ °C/cm$ to $\nabla T_{crit} = 70\ °C/cm$.

A shorter stack corresponds to lower operating temperatures while achieving the critical temperature gradient across the stack. From the data presented, the ideal stack length with respect to resonator length is $\frac{\Delta x_{stack}}{L} \approx 0.07$. The stack placement should be such that the center of the stack is such that $\frac{x_{stack}}{L} \approx 0.20$.

3.6. Orientation effects

A test was done with Design #2 oriented horizontally to evaluate if there is a substantial difference in the cold end temperature. The ice/water cooling was achieved by wrapping a plastic bag around the ice cup to prevent excess dripping, and filling the cooling cup and bag with ice. The average heatup rate of the outside copper of the hot heat exchanger was $1.6\ °C/s$ and the average heatup rate for the cold end was $0.76\ °C/s$.

The temperatures are plotted in Figure 3-12 with the data from the vertically oriented tests for comparison, showing a slightly higher hot temperature at sound onset for the device in the horizontal orientation.

The onset of sound occurred at a lower temperature difference and hot end temperature in the vertical test when compared with the horizontal test. The cold end temperature was also higher in the vertical test.

In the vertical test at sound onset, $T_{hot} = 266\ °C$ and in the horizontal test at onset, this was higher with $T_{hot} = 307\ °C$. These corresponded to $T_{cold} =$

Orientation effects
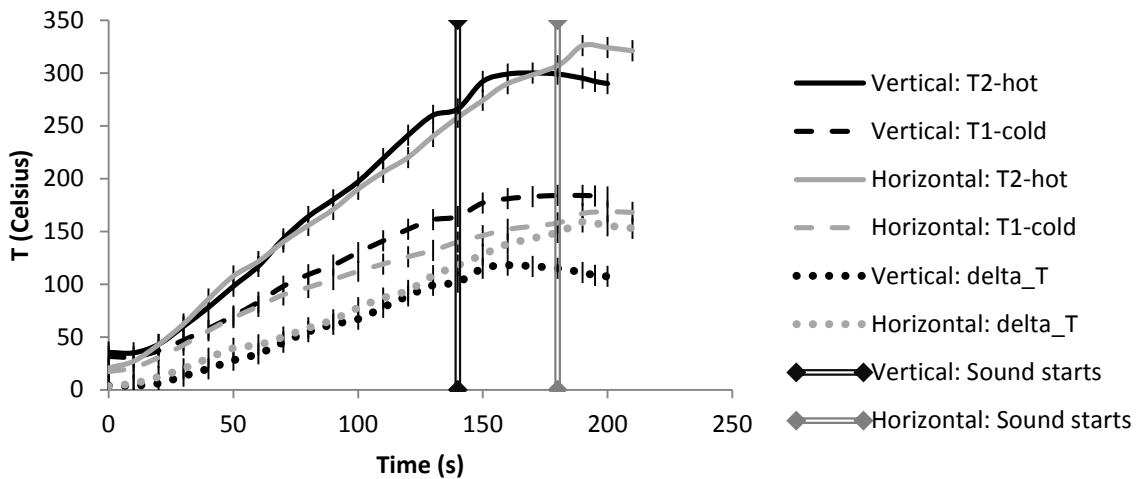
Figure 3-12. Comparison of vertical and horizontal orientations of resonator.

164 ℃ and $T_{cold} = 158$ ℃, and $\Delta T = 102$ ℃ and $\Delta T = 149$ ℃ for the vertical and horizontal orientations respectively. The mean operating temperature was slightly higher for the horizontal orientation, with $T_m = 232$ ℃ compared to $T_m = 215$ ℃ in the vertical orientation. The temperature gradient was also higher in the horizontal orientation, with $\nabla T = 117$ ℃/cm compared to $\nabla T = 80$ ℃/cm in the vertical orientation.

In the vertical orientation, the heat transfers more easily from the hot end to the cold end due to buoyancy assisting gas parcel movement. This contributes to a hotter temperature at the cold heat exchanger, which in turn raises the mean temperature across the stack more quickly. This may explain why the sound occurred at lower hot-end temperatures in the vertical orientation than in the horizontal orientation.

3.7. Sound Analysis

The characteristics of the sound produced by the prototype thermoacoustic flashover detector were measured and analyzed. The sound pressure level ranged from 104 dB at sound onset to a maximum of 122 dB observed in tests. This was evaluated as a function of the increasing hot heat exchanger temperature. The frequency of the sound was estimated for Designs #1 and #2 by comparing the resonator length to published and measured experimental data. The amount of time that the sound continued for was measured and was found to vary from 30 to 90 seconds, based on the rate of heat input and amount of time the heater was left on after the first onset of sound.

3.7.1. Sound Pressure Level

The sound pressure level was measured in decibels by positioning a microphone 38 mm from the open end of the resonator along the x-axis in a test using 62 W on Design #1. The sound increased with increasing temperatures of the hot end. The sound level is plotted as a function of the temperature of the outside of the hot heat exchanger in Figure 3-13**Error! Reference source not ound.**.

The sound started at 104 dB corresponding to $T_{hot} = 304\ °C$. As the power continued to cause an increase in temperature, the sound increased to 120 dB before the power was shut off at $T_{hot} = 336°C$. After this point, the sound continued, with a decreasing intensity until it was gone at 96 dB at $T_{hot} = 296\ °C$.

During this test, the cold end temperature ranged from $T_{cold} = 150 - 160\ °C$ and the temperature difference ranged from $\Delta T = 145\ °C$ at onset to

Sound vs. hot end temperature
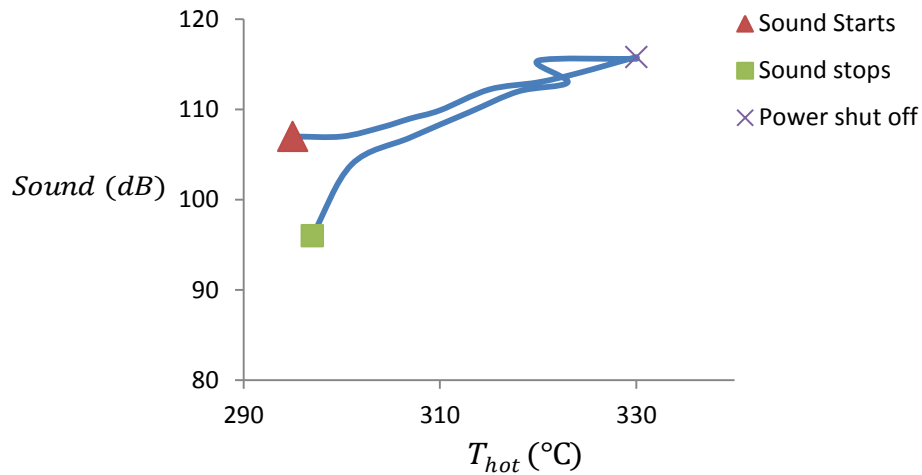
Figure 3-13. Sound vs. hot end temperature, P = 62 W, Design #1.

$\Delta T = 170\ °C$ at the point at which the sound was shut off. It decreased to $\Delta T = 150\ °C$ at the point when the sound stopped.

In another test, the sound reached a level of 122 dB, indicating that the sound has the potential to be louder, depending on the temperatures and power input.

In a fire alarm system, Chapter 18 of NFPA 72 requires that the audible devices have a sound level at least 15 dB greater than the ambient sound level [33]. In this experiment, the ambient sound level was 70 dB, and therefore any audible fire alarm device in the area would need to be at least 85 dB. The measured sound level at onset was significantly louder, at 104 dB measured 38 mm from the device. With the device located on a firefighter's helmet, this level is adequate to alert that firefighter. Further research could analyze sound levels at further distances such that other firefighters or occupants could be alerted from a distance.

3.7.2. Frequency of Sound

The frequency of sound varies based on resonator length, with shorter lengths corresponding to higher frequencies.

The lengths of Design #1 and Design #2 were compared with lengths of the resonator studied by Jung and Matveev as well as the measured frequency of the Pyrex tube resonator to give an estimate of the sound frequency. The frequency data appears to show an exponential trend as shown by the dotted line in Figure 3-14. The frequencies of the prototype of the thermoacoustic flashover detector were fitted into the trend and were estimated to be $f \approx 450\ Hz$ and $f \approx 640\ Hz$ for Designs #1 and #2 respectively.

This sound frequency is distinct from that of a 3000 Hz smoke detector as well as the current safety alarms on firefighters' gear. Furthermore, the frequency
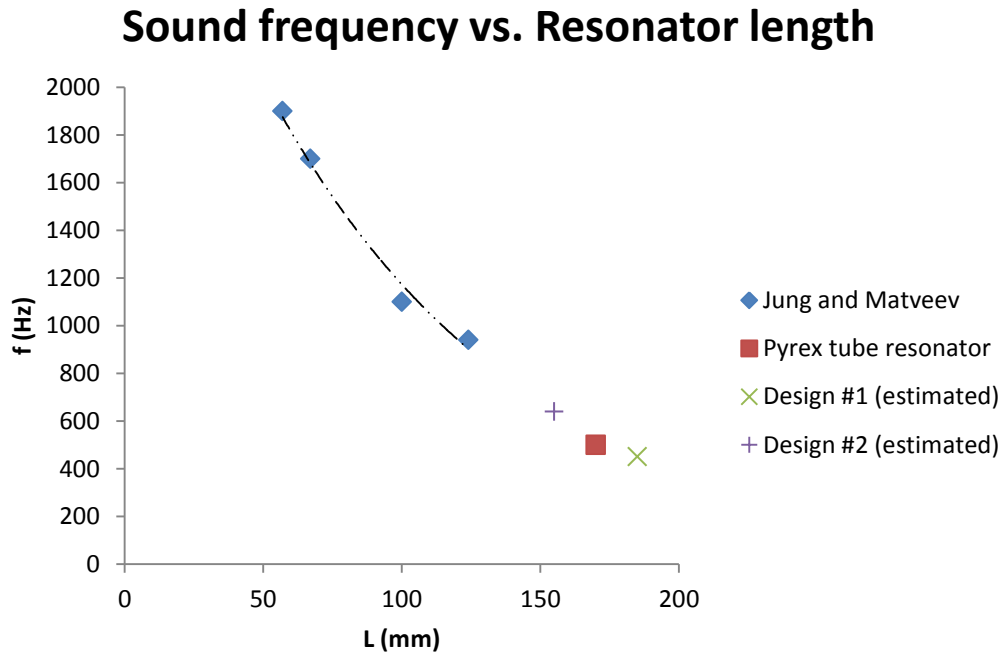

Figure 3-14. Sound frequency vs. resonator length [13].

of 500 Hz is a center frequency and would still be heard by people with some hearing loss.

3.7.3. Sound Continuation

After the onset of sound, the heater was turned off and the sound was able to be sustained for a short period of time which ranged from 30 to 90 seconds.

This sustainment of sound was likely due to the excess energy which was stored in the thickness of the copper foam, passed into the stack. In several of the tests, the power was left on for varying amounts of time post sound onset, ranging from immediate shutoff to 100 seconds. After a certain period of time after power shutoff the sound ceased because there was no energy input to drive the oscillations. The point of sound cessation was also recorded, as well as the heatup rate of the hot heat exchanger in these tests.

The additional continuation of sound after removal of external power is plotted in Figure 3-15. There appears to be a trend for each heatup rate, with the lower heatup rates corresponding to shorter sound continuation lengths and the faster heatup rates corresponding to longer sound continuation lengths. In the plotted tests from Design #2, the device was heated under identical heating conditions and provide a good comparison of the sound length for a given length of power input. This data fits well with the heatup rate of $1.9 \, ℃/s$ from Design #1.

If the heatup rate of $1.9 \, ℃/s$ is considered, the sound continued for 60 seconds upon immediate shutoff, and up to 90 seconds when the power was left on for an additional 30 seconds.

Sound Continuation After Power Shutoff
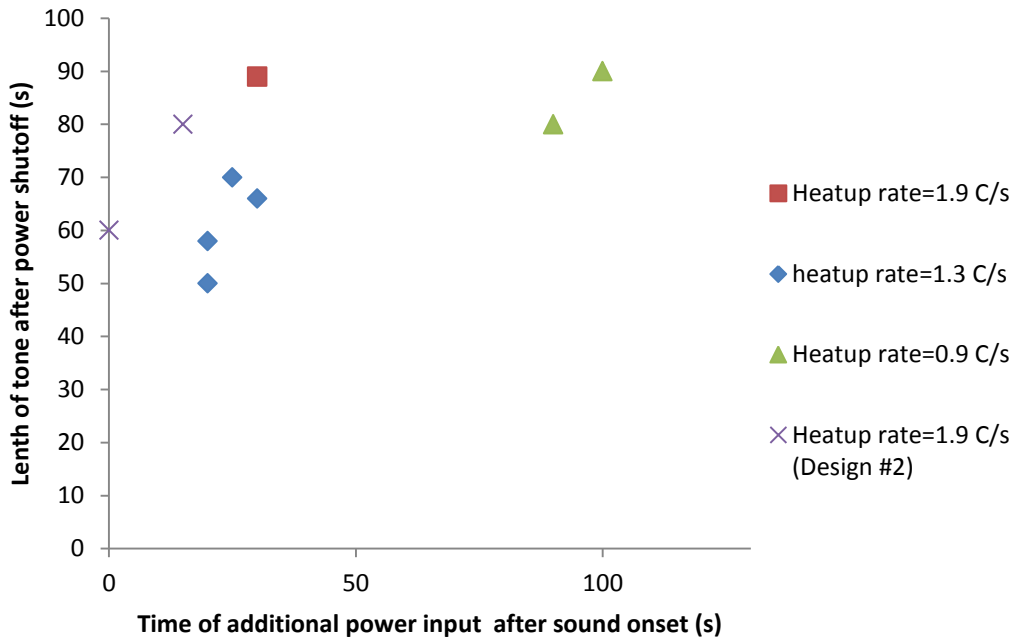
Figure 3-15. Sound continuation after removal of external power.

If the heatup rates of $1.3\ ℃/s$ and $0.9\ ℃/s$ are considered, the sound continued for only 50 seconds with an additional power time of 20 seconds. The sound continued for 90 seconds with an additional power time of 100 seconds.

The copper foam heat exchangers had a larger mass compared to the resistance wire in the Pyrex tube resonator and the copper mesh in the resonator by Jung and Matveev. This additional heat capacity likely increased the amount of time required for the sound to be produced because of the additional mass to be heated up.

The length of the copper foam within the hot heat exchanger translates into a volume of copper which is being heated up inside the resonator adjacent to the stack. Two sizes of hot heat exchangers were used in Design #1 and Design #2, corresponding to $L_{hx} = 12.7$ mm and $L_{hx} = 6.35$ mm, respectively. Using a

74

nominal density of 10% for the copper foam, the volumes of the copper within the two hot heat exchangers were $V_{hx} = 487\ mm^3$ and $V_{hx} = 244\ mm^3$ for Design #1 and Design #2, respectively.

It would be expected that with the smaller volume of the heat exchanger in Design #2, the sound continuation post-power-shutoff would be shorter because of the smaller amount of energy stored in the smaller mass of copper foam. The two tests utilizing Design #2 did here was not a significant difference from this data, but further tests could be done to compare this in more detail.

An even shorter heat exchanger would result in quicker response times given the identical thermal contact with the outside copper ring, which was brazed to the copper foam. For comparison, the resistance wire in the Pyrex tube resonator produced a sound onset within 5 seconds of powering on the power supply, and the sound ceased relatively quickly upon power shutoff as well because of the small mass of the system and almost non-existent power storage. Varying the mass of the copper foam within the hot heat exchanger would have an effect on the response time until sound onset as well as length of sound continuation after removal of external power.

4. Conclusions and Future Work

In the testing on the prototype design of the thermoacoustic flashover detector the critical power input to the hot heat exchanger for steady-state operation after the onset of sound was 31 W, while the critical power needed for sound onset was 44 W. Steady-state was maintained with $T_{hot} \approx 310\,°C$ and $T_{cold} \approx 155\,°C$, corresponding to $\Delta T_{ss} \approx 155\,°C$, $\nabla T_{ss} \approx 78\,°C/cm$ and $T_{m,ss} \approx 217\,°C$. At steady-state, the inside gas temperatures were found to be slightly lower than the hot heat exchanger temperatures so that the heat transfer occurs from the hot heat exchanger to the hot end of the stack to the gas. At the critical power level for sound onset, sound occurred at $\Delta T = 150\,°C$, $T_{hot} = 305\,°C$, $T_{cold} = 150\,°C$, and $T_m = 230\,°C$. The estimated uncertainty in the measured temperatures was $\pm 10\,°C$ and for the power level input was $\pm 5\,W$. Future development will require more precise evaluation of the power input and temperatures, but these measured values provide a foundation and guidelines for future improvement of the device.

The mean temperature across the stack was found to play a role in the onset of sound, shown by lower temperature differences corresponding to higher mean temperatures. Cooling the cold heat exchanger was beneficial, but cooling the temperature of the cold end by $100\,°C$ did not lower the required hot-end temperature. In Design #1, keeping the cold temperature below $60\,°C$ actually caused the hot end temperature at onset to increase from $T_{hot} \approx 300°C$ to $T_{hot} \approx 330°C$. The largest temperature difference at the onset of sound was $\Delta T = 294\,°C$, occurring with the lowest cold heat exchanger temperature and

$T_m = 242\,°\text{C}$, compared to the average temperature difference of $\Delta T = 169\,°\text{C}$ when the cold heat exchanger was not kept this cold and $T_m = 179\,°\text{C}$. This correlation likely occurs because the thermal penetration depth increases with temperature, resulting in more air being heated by the stack at higher temperatures. Further experimentation with a denser steel wool stack may prove to lower the mean temperature at sound onset, allowing for lower temperatures in the device operation. Also, Swift mentioned that the temperatures required are a function of the resonator materials and dimensions, and Symko was able to produce sound with a $40\,°\text{C}$ temperature difference in a 2 cm long resonator by optimizing the device [9, 15].

It was found that the ideal stack position is $\frac{x_{stack}}{L} \approx 0.20$ and the ideal stack length is $\frac{\Delta x_{stack}}{L} \approx 0.06 - 0.12$. From Design #1 to Design #2, $\frac{x_{stack}}{L}$ was reduced from 0.34 to 0.22, resulting in a $34\,°\text{C}$ reduction in temperature difference at the onset of sound. In the Pyrex tube resonator, reducing the stack length from $\frac{\Delta x_{stack}}{L} = 0.15$ to $\frac{\Delta x_{stack}}{L} = 0.09$ resulted in a reduced critical power level for sound onset, from 33 W to 17.8 W.

The orientation of the device appears to have an effect on the heat transfer within the resonator due to buoyancy. A comparison showed that the sound occurred with a $50\,°\text{C}$ lower temperature difference in the vertical test when compared to the horizontal test. This could be due to the higher mean temperature across the stack in the vertical test, compared to the horizontal test. Further tests could be done to confirm the magnitude of this effect on the operation of the device.

The frequency of the sound was estimated to be $\sim 450\ Hz$ for Design #1 and $\sim 640\ Hz$ for Design #2. The current frequency around 500 Hz is ideal to differentiate from the higher 3000 Hz frequency of smoke detectors. Furthermore, this is a center frequency that is easily heard. As the length of the resonator decreases, the frequency increases. In future modifications, the resonator should be designed to best obtain the firefighter's attention during the impending flashover. The tone should also remain distinct from any other device on the firefighter's apparatus.

The power and temperatures needed for the onset of sound are highly dependent on the geometry and materials of the device and can be optimized by selecting the best stack position, device dimensions and materials [9].

The design for the resonator should be a cylinder with a length-to-inner diameter ratio in the range of 8 to 50 [16]. With the total inside length including gaskets, these ratios were $\frac{L}{ID} = 9$ for Design #1 and $\frac{L}{ID} = 7.3$ for Design #2. This suggests that the inner diameter could be made smaller in future designs. It is not known if changing this ratio affects the operating parameters of the device, but this could be explored in future research and experimentation.

Minimizing the thermal and viscous losses of the oscillating gas within the resonator should have an optimizing effect on the device. It is important to keep in mind the thermal and viscous boundary layer depths for the gas, which are on the order of 0.1 mm. Using a material with a surface roughness larger than these boundary layer depths could hinder the gas oscillations, requiring more power for the gas particles to oscillate enough to produce a sound wave. This would in turn

require more power for the device to operate and produce sound. It is ideal to produce the sound with as little power and heat as possible, therefore the material used for the resonator should have a very smooth inner wall and the junctions of the heat exchangers with the resonator should be as smooth as possible to minimize any slowing down of the gas parcels as they oscillate. The resonator and heat exchangers could be a composite with smooth junctions brazed or soldered together.

The cold end of the resonator simply needs to be a tube to fit in the assembly. The aluminum pipe nipple worked well, was easily machinable using a lathe, and fit into the threaded flange on the end, allowing the opening end to remain open for the sound to propagate from. Because the length of this piece will affect the overall resonator length, the frequency of the sound will vary as well.

The cap on the closed end should be an insulating material to minimize heat losses to the atmosphere. This end also becomes hot due to the heat input to the adjacent hot heat exchanger, so it would be desirable to keep this portion insulated upon implementation in a firefighter's helmet or gear. The inner surface should be smooth to minimize viscous losses during the pressure and velocity gas oscillations. To allow simpler heat input to the device from the outside, further designs could experiment with reduction in the length of this cap. This introduces the concept of replacing the end cap with the hot heat exchanger while maintaining $\frac{x_{stack}}{L} \approx 0.20$.

The portion of the device holding the stack should also be an insulating material. The purpose of this section is to prevent heat from being transferred

from the hot heat exchanger to the cold heat exchanger along the wall of the tube. The heat transfer within this section should be in the x-direction along the direction of sound wave propagation, not in the y-direction. This will establish a steeper temperature gradient given a power input. This insulating material could be ceramic or Teflon, depending on the temperatures anticipated.

Macor machinable ceramic was a very good choice for the cap and stack holder because of its low thermal conductivity high melting temperature. Macor can be continuously subjected to 800℃, although temperatures this high are not anticipated in the device. This material is non-porous and can be machined carefully using carbide tools [25]. The downside to this material is that it can be brittle and care must be taken during handling. This material proved to work successfully and repeatedly in tests. It has properties similar to glass, the resonator material used in the Pyrex tube resonator by Baz et al., which this design was initially based upon.

In future designs, Teflon PFTE (polytetrafluoroethylene) would be a good choice for the cap and stack holder because it is an insulating material and thus will not contribute very much to heat conduction along the resonator from the hot to cold heat exchanger. It is also easily machinable and a relatively durable material, but begins to break down at 260 ℃ and melts at 327 ℃ [27].

The device design worked successfully with Teflon for the cap and stack holder, but the operating temperature at the hot end was ~316 ℃. Unfortunately the Teflon deformed and these tests were not repeatable. Future optimization of

the device and reduction in operating temperatures to below 260 ℃ would make Teflon a good material for the cap and stack holder.

The coefficient of thermal expansion is important to consider when joining together different materials to be heated up. The coefficients are listed in Table 4-1 for the materials under consideration in the resonator.

Material	Coeff. Of Thermal Expansion (m/m℃)
Copper	$1.70 * 10^{-5}$
Teflon PTFE	$1.35 * 10^{-4}$
Macor ceramic	$9.30 * 10^{-6}$
Pyrex glass	$4.00 * 10^{-6}$
Stainless Steel (316)	$1.60 * 10^{-5}$

Table 4-1. Coefficients of expansion for materials under consideration.

From the coefficients of thermal expansion listed above, it can be noted that the Teflon expands ~ 10 times more than the copper. This explains why in preliminary designs with copper inside Teflon at junctions, the copper slipped out when heated up. Therefore if Teflon is to be used as a stack holder or cavity, it should be slightly inside the copper at the junction of copper to Teflon. Then as both the copper and Teflon heat up, the Teflon will expand into the copper and make the seal even tighter.

The stainless steel and copper have very similar coefficients of thermal expansion, within 10^{-6} of eachother, indicating that these may be good choices to bond together when subjected to high temperatures. However, the stainless steel does not act well as an insulator for the stack holder and is not a strong choice because of conduction along the x-direction from the hot to cold heat exchangers.

The heat would then convect inward, heating up the air within the stack more uniformly and reducing the temperature gradient within the stack along the x-direction.

The Macor ceramic has a smaller coefficient of thermal expansion than the copper, but may be subject to cracking if the copper is inside the Macor and pushes outward. Therefore the Macor in the prototype design tested was designed to fit slightly inside the copper at the joint. Therefore the expansion of copper during heatup did not push outward on the ceramic, which can be brittle. Pressing a high-temperature graphite gasket between the copper and Macor junction successfully sealed the joint.

The stack used was a steel wool cylinder with fiber thicknesses of about 0.1 mm and a density of $\rho_{stack} = 156 \ kg/m^3$. This was initially chosen because it performed successfully in the Pyrex tube resonator and was easily machinable by hand to conform to the inside of the resonator. The stack was pushed up against the heat exchangers so that the hot and cold end temperatures were anchored to produce a temperature gradient across the stack.

The stack should be a porous material with a high heat capacity and low thermal conductivity, to provide heat capacity for the gas [8]. By minimizing the gap between the stack and the walls to a distance on the order of the thermal boundary layer thickness, the stack is able to influence more of the working gas to produce oscillations [8]. Likewise, the porosity of the stack should be such that the distance between fibers or parallel plates is on the order of $2\delta_K$, where $\delta_K \approx 0.17 - 19 \ mm$ and increases with increasing temperature.

In future designs, the stack could be alternate materials or densities such as such as different steel wool grades, parallel plate spirals, ceramic or metal honeycomb. Increasing the density of the stack will most likely reduce the operating temperature needed for the onset of sound. This could be evaluated by testing identical resonator designs with different stacks.

The thickness of the copper foam heat exchanger, $L_{hx,hot}$, will have an influence on the time to sound onset as well as the amount of time for which the sound will continue with the external heat source removed. Larger dimensions for $L_{hx,hot}$ will likely require longer heatup times before the onset of sound, but the sound will continue for a longer period after the external power input is shut off. The effect of varying this dimension could be analyzed in identical resonators while varying only this component.

In further development, the cold heat exchanger could be kept at a more constant temperature by embedding cooling within the device. Instead of the cold heat exchanger consisting of copper foam being cooled from the outside only, more efficient cooling could be achieved by running cold water lines through the cold heat exchanger. This could be through tiny fins, parallel plates, or heat pipes. The water in these lines could carry heat from the inside of the device to the outside, providing a more efficient way to thermally anchor the cold end. Cooling could also be achieved by submerging the cold heat exchanger in Rubitherm PX 50. This is a powder which melts at $49 - 51°C$ with a specific heat capacity of $1.6 \, kJ/kgK$. It is composed of silicone dioxide and has a maximum operating

temperature of 70 ℃. The airflow from the respirator in the firefighter's gear could serve as a source of cooling in the ultimate design.

The entire resonator device must be airtight, with the exception of the circular hold at the open end through which the sound propagates. Eliminating air leaks ensures that the gas particles will be able to oscillate at pressures and velocities that produce the sound wave. Any leakage of air prevents the pressure from building up, which in turn prevents the sound from being produced. This was confirmed in experiments and the compression via flanges and graphite gaskets proved to be adequate.

5. References

[1]   National Fire Service Research Agenda Symposium, National Firefighters
        Foundation, Emmitsburg, Maryland (2005).
[2]   Walton, William D. and Thomas, Philip H., "Estimating Temperatures in
        Compartment Fires," SFPE Handbook, 3rd Edition, National Fire
        Protection Association, Battery Park, 2002.
[3]   Society of Fire Protection Engineers, SFPE Handbook, 3rd Edition,
        National Fire Protection Association, Battery Park, 2002.
[4]   Purser, David A., "Toxicity Assessment of Combustion Products," SFPE
        Handbook, 3rd Edition, National Fire Protection Association, Battery
        Park, 2002.
[5]   Karlsson, Bjorn and Quintiere, James G., Enclosure Fire Dynamics, CRC
        Press LLC, Boca Raton, 2000.
[6]   ISO Glossary of Fire Terms and Definitions, International Standards
        Organization, Geneva, 1996.
[7]   Rossing, Thomas D., "Thermoacoustics," Springer Handbook of
        Acoustics, Springer Media LLC, New York, 2007.
[8]   Swift, Greg., Thermoacoustics: A unifying perspective for some engines
        and refrigerators, Fifth draft, Los Alamos National Laboratory, 2001.
[9]   Swift, G. W., "Thermoacoustic engines," J. Acoust. Soc. Am., Vol. 84,
        No. 4, pp. 1161-1165, 1988.
[10]   Symko, Orest G ., "Energy conversion using thermoacoustic devices,"
        18th International Conference on Thermoelectrics, 1999.
[11]   Babaei, Hadi and Siddiqui, Kamran, "Design and optimization of
        thermoacoustic devices," Energy Conservation and Management, Vol. 49,
        pp. 3585-3598, 2008.
[12]   Backhaus, Scott and Swift, Greg, "New Varieties of Thermoacoustic
        Engines," Condensed Matter and Thermal Physics Group, Los Alamos
        Laboratory, Presented at 9th International Congress on Sound and
        Vibration, July 2002.
[13]   Jung, S and Matveev, K I, "Study of a small-scale standing-wave
        thermoacoustic engine," Journal of Mechanical Engineering Science, Vol.
        224, 2009c.
[14]   Dry air properties. Engineering toolbox. [Online]
        http://www.engineeringtoolbox.com/dry-air-properties.
[15]   Symko, O. G., Abdel-Rahman, Kwon, Y.S., Emmi, M., Behunin, R.,
        "Design and development of high-frequency thermoacoustic engines for
        thermal management in microelectronics," Microelectronics Journal, Vol.
        35, pp. 185-191, 2004.
[16]   Carter, R. L. and Feldman, K. T., "A Study of Heat Driven Pressure
        Oscillations in a Gas," Journal of Heat Transfer, pp. 536-540, August
        1970.
[17]   Chinn, Daniel George, "Piezoelectrically-driven Thermoacoustic
        Refrigerator," Ph.D. Dissertation, University of Maryland, College Park,
        2010.

[18]   Wheatley, J., Hofler, T., Swift, G.W., Migliori, A., "Understanding some simple phenomena in thermoacoustics with applications to acoustical heat engines," American Journal of Physics, Vol. 53, pp. 147-162, 1985.

[19]   PHYSorg.com, "A sound way to turn heat into electricity." [Online] June 4, 2007. http://phys.org/news100141616.html.

[20]   NASA, Temperature Scales and Absolute Zero, Cryogenics and Fluids Branch. [Online] September 9, 2004. http://cryo.gsfc.nasa.gov/introduction/temp_scales.html.

[21]   Smoker, J., Nouh, M., Aldraihem, O., Baz, A., "Energy harvesting from a standing wave thermoacoustic piezoelectric resonator," J. Appl. Phys. 111, 104901 (2012).

[22]   McLaughlin, Bonnie Jean. "Study and development of high-frequency thermoacoustic prime movers with piezoelectric transducers," Ph.D. Dissertation, The University of Utah, 2008.

[23]   Omega. 1-Piece Mica Insulated Band Heater. [Online] Omega Engineering, Inc., 2012. http://www.omega.com/pptst/MB-1_HEATER.html.

[24]   Duocel Copper Foam. ERG Aerospace Corporation. [Online] 2011. http://www.ergaerospace.com/Copper-properties.htm.

[25]   Corning, Glass Ceramic - MACOR Machinable glass ceramic. [Online] 2012. http://www.corning.com/specialtymaterials/products_capabilites/macor.aspx.

[26]   McMaster Carr, Gaskets. [Online] http://www.mcmaster.com/#flange-gasket-rings/=i2yleb.

[27]   Engineers Edge, Fluoropolymer Comparison - Typical Properties, DuPont. [Online] http://www2.dupont.com/Teflon_Industrial/en_US/tech_info/techinfo_compare.html.

[28]   Engineers Edge, Properties of Metals. [Online] http://www.engineersedge.com/properties_of_metals.htm.

[29]   Strutt, J. W. and Baron Rayleigh, "The explanation of certain acoustical phenomena," Nature, Vol. 18, pp. 319-321, 1878.

[30]   Nouh, Mostafa, "Thermoacoustic-piezoelectric systems with dynamic magnifiers," Ph.D. Dissertation, University of Maryland, College Park, 2012.

[31]   Feldman, K. T., "Review of the literature on Sondhauss thermoacoustic phenomena," Journal of Sound and Vibrations, Vol. 7, 1968.

[32]   Matveev, Konstantin I., "On the coupling between standing-wave thermoacoustic engine and piezoelectric transducer," ASME, Seattle, 2007.

[33]   NFPA 72 *National Fire Alarm and Signaling Code*, 2010. NFPA, Quincy, MA.